Nanoscale

Accepted Manuscript

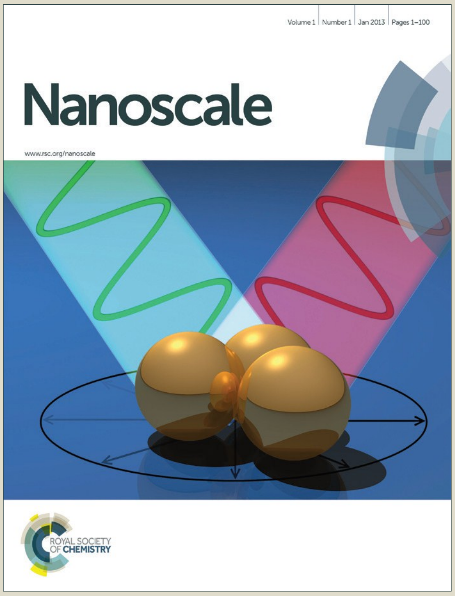

ROYAL SOCIETY OF CHEMISTRY

www.rsc.org/nanoscale

Nanoscale

ARTICLE

Integration of Inorganic Nanostructures with Polydopamine-Derived Carbon: Tunable Morphology and Versatile Applications

Received 00th January 20xx,
Accepted 00th January 20xx

DOI: 10.1039/x0xx00000x

www.rsc.org/

Junhua Kong,[a] Seyed Ismail Seyed Shahabadi,[a] Xuehong Lu[a,]*

Polydopamine (PDA), a mussel adhesive-inspired biomimetic polymer, has attracted tremendous attention owing to its extremely versatile adhesion properties, facile aqueous coating process, capability of self-assembly to form nanostructures, and abundant surface functional groups for secondary modification. PDA is also a fantastic carbon source because it gives nitrogen (N)-doped graphite-like carbon at high yield, and the carbonized PDA (C-PDA) thin coatings have similar properties to that of N-doped multilayered graphene, i.e., exhibiting high electrical conductivity, good electrochemical and mechanical properties. In comparison with other carbon sources, an outstanding feature of PDA lies in its ease of integration with inorganic nanostructures and capability for easy tailoring the structure and morphology of the resultant composite nanostructures. In this article, different routes for preparation of C-PDA-based composite nanostructures, such as carbon/metal oxide and carbon/Si hollow, mesoporous, core-shell, yolk-shell nanostructures, are introduced with typical examples. The structures, morphologies and properties of the C-PDA-based composite nanostructures are also reviewed, and their potential applications in various engineering fields, such as energy storage, solar water splitting, flexible electronics, catalysis, sensing and environmental engineering, are highlighted. Finally a future outlook for this fascinating composite-nanostructure enabler is also presented.

1. Introduction

As one of the most versatile materials, carbon has found wide uses in many fields, such as energy harvest/storage, sensing, catalysis and environmental science, mainly due to its extraordinary properties, including low density, high thermal and electrical conductivity, good chemical and electrochemical stability, and excellent mechanical strength for some carbon allotropes. Carbon is also frequently integrated with inorganic nanomaterials to form nanocomposites. By synergistically combining the properties of carbon and inorganic phases, carbon-based nanocomposites offer rich possibilities for developing novel high-performance functional or multifunctional materials. To fabricate a carbon-based nanocomposite with desired properties for a targeted application, carbon source must be appropriately chosen since it directly influences the structures, morphology and properties of the carbon phase. The type of carbon source would also determine the processing routes for the carbon-based nanocomposites, which affect the interfacial interactions between the carbon and inorganic phases and ultimately the properties of the nanocomposites. Common types of carbon source, including small molecules, renewable compounds, and polymers, have been well summarized in recent review articles.[1-10] This review will focus on a unique carbon source, polydopamine (PDA), which is an ideal candidate for integration of carbon with inorganic nanostructures. PDA can be easily converted to a special category of carbon, nitrogen-doped (N-doped) graphitized carbon. The graphitization of the carbon benefits both in-plane and through-plane electrical conduction, while the internal doping with quaternary nitrogen is in favour of electrons transport thus further improvement of electrical conduction.[11] The doping also induces structural disorder and defects into carbon that frequently leads to enhanced electrochemical activity. N-doped carbon can be produced from many types of carbon sources and through different routes, which have been introduced in a number of reviews.[12-15] The outstanding feature of PDA as the source of N-doped graphitized carbon lies in its ease of integration with inorganic nanostructures and capability for easy tailoring the morphology of the composite nanostructures, as well as the possibility for facile secondary modification. In the following sections of this review, structures and properties of PDA and carbonized PDA (C-PDA) will be introduced firstly, and then various strategies used for fabrication of C-PDA nanostructures and C-PDA-based composite nanostructures will be presented with typical examples. The potential applications of these composite nanostructures in various fields will also be highlighted.

2. Structures and properties of polydopamine

---

[a] School of Materials Science and Engineering, Nanyang Technological University, 50 Nanyang Avenue, Singapore 639798.

PDA is a mussel adhesive-inspired biomimetic synthetic polymer with good affinity to almost any solid surface through chemical binding and physical interactions resulting from its diverse functional groups, especially its catechol group. In general, there are three routes to prepare PDA, i.e., enzymatic catalytic oxidation,[16] electrochemical polymerization (on electrically conductive electrode),[17] and oxidation polymerization in solutions. Enzymatic catalytic oxidation is an effective route for PDA synthesis.[18] In the presence of laccase and under pH of about 6, dopamine can be oxidized and then polymerizes into PDA. In this case, the catalyst, laccase, is finally encapsulated in the formed PDA as impurities. This may bring deleterious effect to the properties of PDA. Pure PDA thin films can be prepared via electrochemical polymerization of DOPA. The polymerization is carried out by cyclic voltammetric process using deoxygenated phosphate buffer solution that contains o-phenylenediamine, dopamine and L- or D-glutamic acid as electrolyte. Films with large and adjustable thickness can be achieved through the electrochemical route. However, it can only be formed on electrically conductive substrates, gold electrode for instance. Compared with the above two, solution oxidation is the most popular method because the oxidation polymerization of dopamine (DOPA, Fig. 1a) can be conveniently conducted at room temperature in basic aqueous solutions, forming PDA coating on various substrates.[19] Despite the diverse preparation routes, the polymerization mechanism and resultant PDA structure is still not fully clarified up to date. Nonetheless, it is widely accepted that multiple reactions and conversions, including oxidation of dopamine into dopamine-quinone, intramolecular cyclization, rearrangement, further oxidation into indole-quinone, are involved during the polymerization.[20-23] The complicated process leads to structural diversity and disorder, which are significantly dependent on the monomer concentration, buffer type, pH value, and the oxidant used.[21, 24, 25] At the early stage of the structure investigation, it was believed that the dopamine monomers were oxidized, cyclized and then covalently joined together via aryl-aryl or other chemical bonding (Fig. 1b).[19, 26] F. Bernsmann et al. suggested in 2011 that the formation of PDA resembles the pathway of synthetic melanin.[25] The oxidation of dopamine forms 5,6-dihydroxyindole and then 5,6-indolequinone. These two molecules undergo further branching reactions at positions 2, 3, 4 and 7, resulting in multiple isomers of dimers and higher oligomers that finally self-assemble into PDA (Fig. 1c). Later on, D. R. Dreyer et al. confirmed the supramolecular aggregate of monomers that are held together through charge transfer, π-π stacking and hydrogen bonding, rather than simply covalent bonding, during the formation of PDA (Fig. 1d).[27] The spacing between the stacked layers is about 0.38 nm as verified by X-ray diffraction spectroscope (XRD). It is worth mentioning here that the stacked layers can also be directly observed under high-resolution transmission electron microscope (HRTEM), and the interlayer spacing is measured to be around 0.40 nm.[28] This further confirms the stacking mechanism. S. Hong et al. then proposed that the formation of PDA involves both the covalent bonding between the units (top and bottom black structures in Fig. 1e) and the non-covalent self-assembling of monomers or formed oligomers such as aromatic rings stacking on each other (red, blue and middle black structures in Fig. 1e), leading to a typical structure of PDA as shown in Fig. 1e.[22]

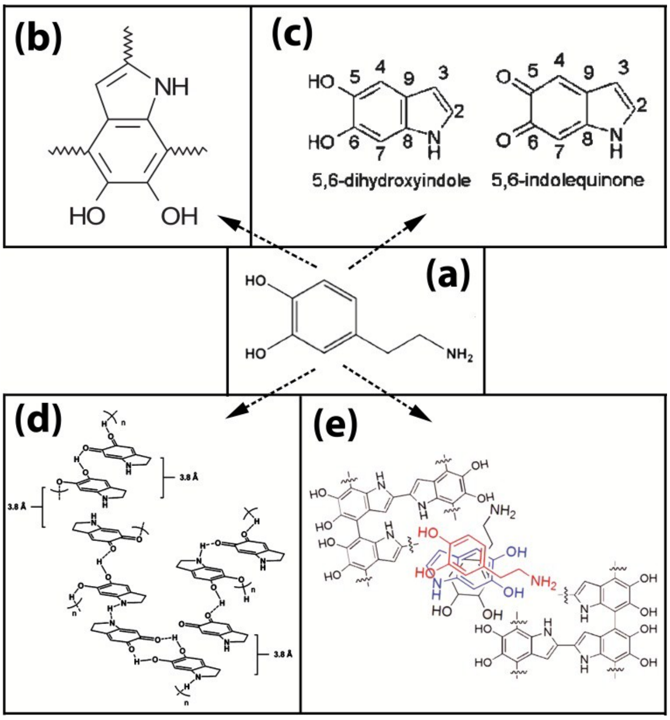

Fig. 1 (a) Chemical structure of DOPA monomer, (b-e) proposed chemical structures of PDA by different research groups [figure (b): reprinted with permission from ref. [26]. Copyright 2010, Elsevier; figure (c): reprinted with permission from ref. [25]. Copyright 2011, American Chemical Society; figure (d): reprinted with permission from ref. [27]. Copyright 2012, American Chemical Society; figure (e): reprinted with permission from ref. [22]. Copyright 2010, John Wiley and Sons].

PDA is a biocompatible and biodegradable polymer,[29, 30] and has strong ultraviolet (UV)-visible-NIR light absorption and weak fluorescence upon excitation by UV light, which is due to its chemical disorder.[31, 32] In terms of electronic properties, PDA resembles either amorphous organic semiconductors[33, 34] or electronic-ionic hybrid conductors[35] due to the π-system, leading to electrical conduction capability which is critically affected by temperature, morphology and environmental humidity. PDA owes its paramagnetism property to the stable π-electron free radical species,[36] and its chemical activity to functional groups. It is capable of reacting with a wide variety of molecules, such as amine, thiol- or carboxyl-containing compounds, and 1,3,5-benzenetricarbonyl trichloride.[37-39] Moreover, the catechol groups in PDA are able to reduce noble metal ions, including Ag^+, Au^{3+}, and Pt^{3+}, to corresponding metals as they are oxidized into quinone groups upon the release of electrons and protons.[40-42] Mimicking mussel adhesive proteins, PDA is also capable of forming complexes with various transitional metal ions, such as Fe^{3+}, Mn^{2+}, Ni^{2+}, and Co^{2+},[43-49] due to its diverse functional groups, especially catechol group which enables coordination bonding between PDA and the metal ions. The types of the complexes formed are strongly dependent on the solution pH value.[50, 51] Last but not least, PDA exhibits fairly good thermal stability and chemical resistance to organic electrolytes and physiological buffers, which renders itself a good candidate as protective coating in the areas of sensing and energy.[52]

PDA is a promising carbon source owing primarily to its strong affinity to various types of solid surfaces, which enables facile formation of PDA thin coatings on a wide variety of organic and inorganic substrates. When it is coated on inorganic nanostructures, the conversion of PDA coating to C-PDA coating alters the surfaces of the inorganic component thus leads to C-PDA-based composite nanostructures with improved or new functionalities. The thickness of PDA coating can be facilely controlled. In addition, the abundant functional groups in PDA, including catechol, amine, and imine, allow it to covalently link with other organic molecules or chemically bridge with a wide variety of transition metal species. This offers rich opportunities to further modify PDA coating and consequently bring about numerous novel hybrid materials with unique structures and properties. The aqueous preparation route and relatively high carbon yield of PDA (~60 wt%) upon annealing in inert environment also render it an environmental friendly and cost-effective carbon source.

3. Structures, properties, and morphology of polydopamine-derived carbon

3.1 Chemical structures and properties of polydopamine-derived carbon

Like most other polymeric precursors, pyrolysis is the major process to obtain carbonaceous materials from PDA. Simple carbonization at high temperatures, normally above 700 °C, in inert environment, with flowing argon for instance, converts PDA to C-PDA with complicated chemical reactions and physical changes involved. Nevertheless, the chemical structure and physical properties of C-PDA differ from those of other carbon sources due to the unique structure of PDA. In 2011, Dai et al. thermally converted solution oxidation-derived PDA to carbon at 800 °C in N_2 successfully for the first time.[54] The carbon is doped with about 7.28 wt% nitrogen, using the above carbonization condition,[55] and the carbon yield is nearly 60 wt%. It had been suggested that PDA is similar to melanin in structure, which is composed of stacked oligomeric proto-molecules with indolequinone units,[56, 57] and it is highly possible that the derived carbon would resemble the layered structure of its precursor. Thus, we investigated the structure of PDA, which was in thin film form and fabricated on oxidized silicon wafer.[28] HRTEM, Raman spectroscope, XRD, X-ray photoelectron spectroscope (XPS), as well as Fourier transform infrared spectroscope (FTIR) were used to study the structure. The results show that the C-PDA coating obtained indeed has layered structure with interlayer spacing of 0.37 nm (Fig. 2a), which well resembles that of uncarbonized PDA film that has a slightly larger interlayer spacing (0.40 nm). The layered structure was further confirmed by the XRD results, where a single diffraction peak at about 22 º for both PDA and C-PDA coatings was observed, which verifies the graphite-like layered structure. Nevertheless, the structural order is significantly improved after carbonization with the increase of crystal size from 2.0 nm for PDA to 5.3 nm for C-PDA, despite that there are still considerable amount of defects in the carbon. The XPS spectrum shows that the carbon is doped with 6.7 wt% and 4.5 wt% of oxygen (O) and nitrogen (N), respectively, under the carbonization temperature of 700 °C in argon, indicating that N and O are only partially removed. The carbonized PDA thin coating can therefore be regarded as multilayered graphite

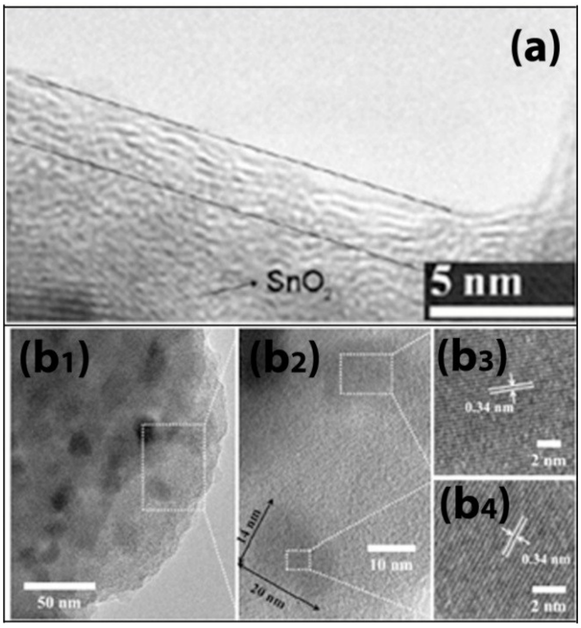

Fig. 2 (a) Layered structure of C-PDA coating formed on SnO_2 aggregates [reproduced from Ref. [28] with permission from the Royal Society of Chemistry], (b_1~b_4) C-PDA nanoparticles that have graphite domains dispersed in amorphous matrix [reprinted with permission from ref. [53]. Copyright (2014) American Chemical Society].

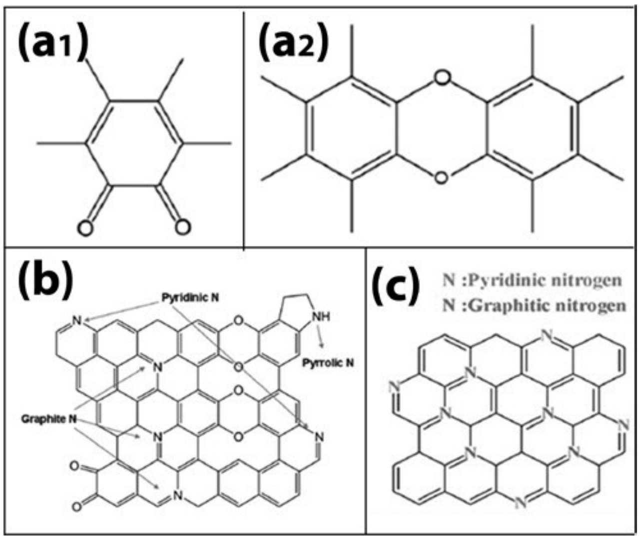

Fig. 3 Chemical structure of C-PDA proposed by (a_1 and a_2) Kong et al. [reproduced from Ref. [28] with permission from The Royal Society of Chemistry], (b) H. Li et al. [reproduced from Ref. [58] with permission from The Royal Society of Chemistry], and (c) K. Ai et al [reprinted with permission from ref. [59]. Copyright 2012, John Wiley and Sons].

doped with heteroatoms. This was further supported by the ordered hexagonal diffraction patterns and/or diffraction rings from the selected area electron diffraction (SAED) results reported by Mullen's group.[60] The structural study of C-PDA particles prepared under carbonization temperature of 800 °C in N_2 by Jin's group in 2014, however, showed slightly different results; the C-PDA particles have an amorphous carbon matrix embedded with graphite-like domains of size of about 15 nm (Fig. $2b_1$~b_4).[53] Several domains containing a few ordered stacking layers were also observed. Regarding the chemical structure of C-PDA, our XPS study revealed that the doped N in C-PDA thin film is further divided into around 46.5 wt% pyridinic N, 52.5 wt% pyrrolic N, and 1.0 wt% graphitic N.[61] The FTIR analysis shows that PDA is partially cross-linked via C-O-C bonds during carbonization, while some catechol groups may be converted to conjugated C=O and some N atoms are also present in the cross-linked structure (Fig. $3a_1$ and a_2).[28] This is further supported by the analysis by H. Li et al., which showed that the structure of PDA is transformed to N-doped carbon that is partially cross-linked via C-O-C bonds after carbonization (Fig. 3b).[58] The cross-linking helps to retain the multilayered structure of PDA, while the removal of heteroatoms (N, O and H) may bring the layers closer to each other, from 0.40 nm to 0.37 nm as aforementioned. Differently, K. Ai et al. claimed that the doped-N in C-PDA sub-micrometer spheres obtained by annealing at 800 °C in argon is composed of 69.72 % graphitic N and 30.28 % pyridinic N with a chemical structure shown in Fig. 3c, and the C is mainly in sp^2 state.[59] The variation of chemical structures of C-PDA reported by different research groups may be due to the different polymerization conditions used that lead to structural variation of PDA. In the first case (reported in ref. 28, 58 and 61), the polymerization was carried out in conventional aqueous environment using tris(hydroxymethyl) aminomethane (Tris) as the buffering agent, whereas in the case reported in ref. 59, the polymerization was carried out in the mixture of deionized water, ethanol and ammonia. The polymerization condition reported in ref. 59 results in spherical morphology, for which the size can be adjusted by altering the ammonia amount, while it may also alter the chemical structure of PDA and hence the structure of C-PDA. Moreover, although oxygen atoms have been detected in the C-PDA samples reported in ref. 59, only N and C were taken into consideration concerning the chemical structure of C-PDA. Therefore the proposed structure in ref. 59 may only partially reflect the true structure of C-PDA.

Besides the pyrolysis of PDA to obtain carbon, the hydrothermal treatment of dopamine at high temperature of 180 °C could also yield C-PDA.[62] The derived carbon has sp^2 graphitic structure with the existence of phenolic hydroxyl carbons, indole/pyrole unit carbons, aliphatic carbons, and carbonyl carbons. The lattice spacing is 0.325 nm and close to [002] interlayer spacing of graphite. It is also shown that the surface of the carbon is rich in indole/indoline units and hydroxyl groups, offering hydrophilicity and hence the ability for the carbon to be stably and homogeneously suspended in aqueous media. In terms of property, the derived carbon dots exhibit broad emission spectra ranging from 380 nm to 530 nm, depending on the excitation wavelengths; for instance, blue-green photoluminescence was observed under excitation of ultraviolet light.

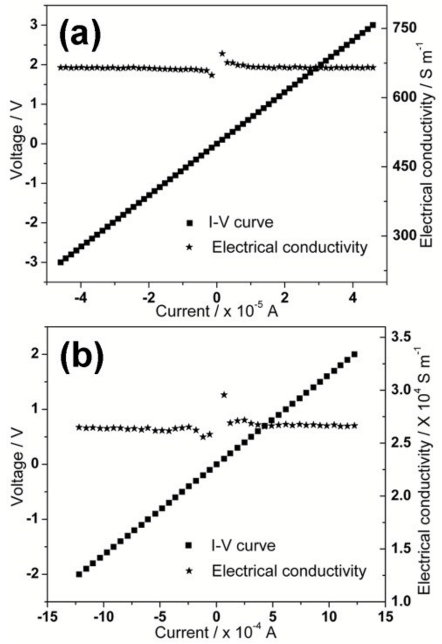

Fig. 4 The electrical conductivity of C-PDA coating (a) in and (b) through the basal plane [reproduced from Ref. [28] with permission from The Royal Society of Chemistry].

High electrical conductivity is one of the most significant properties for C-PDA. Although the C-PDA coating has more defects than the multilayer graphene prepared from other carbon sources, the in-plane and through-plane electrical conductivities (the latter was measured on a FTO substrate) of the C-PDA coatings prepared by annealing at 700 °C are about 660 and 26,600 S m^{-1}, respectively (Fig. 4), which are comparable to those of multilayer graphene.[28] The high conductivities obtained may be attributed to the altered molecular charge-transfer behaviour induced by the n-type doping by nitrogen and effective π-π stacking. Mullen et al. showed that the electrical conductivity of C-PDA film is highly dependent on the carbonization temperature while independent on the film thickness within the range of 3.4 – 20.5 nm.[60] For instance, the average in-plane conductivity is as high as 1200 S cm^{-1} when the treatment temperature is 1000 °C. They also found that the resistance of the film increases linearly with the stretching rate from 0 % to 20 %, and it rebounds back to the original value when the stretching is removed. In their experiments, the C-PDA film was attached onto plastic substrate (polydimethylsiloxane, PDMS), and stretched in one direction using external force. The stretching rate was defined as the ratio of increased length to original length (in the direction of stretching). The resistance-stretching relationship is recyclable, indicating the great flexibility of the film and the potential application as flexible, transparent electrode. The high conductivities greatly benefit charge transport, which is critical for electrochemical and some other applications that involve electrical conduction.

3.2 Morphology of polydopamine-derived carbon nanostructures

Of different types of C-PDA nanostructures, C-PDA thin film/coating is the most studied one. Highly stretchable and conductive carbon film was obtained by coating PDA onto oxidized silicon (SiO_2/Si) wafer or Cu foil.[28, 60] Typically, the substrate was simply immersed into aqueous solution of dopamine in the concentration range of 0.3 – 2.0 mg/mL in the presence of Tris (pH = 8.5). PDA coating was readily formed on the substrate and then went through an annealing process to be converted to C-PDA film, which was still well adhered to the substrate without any obvious cracks or peeling. The surface of the film is fairly smooth with low surface roughness (~ 0.60 nm). The thickness of the carbon film is adjustable from several nanometers to tens of nanometers, depending on the monomer concentration, polymerization duration, and the number of times the coating procedure was repeated. The size of the carbon film can be as large as that of silicon wafer. Using a fast and contamination-free "direct dry-transfer" method developed by Mullen et al.,[60] the PDA film deposited on Cu foil could be facilely transferred onto plastic substrates that possess low surface energy, e.g., PDMS. In this method, the van der Waals force is the driven force to "attract" the carbon film. Without using any substrate, C-PDA with layered microstructure can also be attained. X. Liu et al. reported that micro/mesoporous nitrogen-doped carbon multilayer assemblies could be prepared without any substrate and buffering agent.[63] To achieve this, dopamine and $FeCl_3$ with mass ratio of 1:5 were mixed and pressed together, and then heated to a certain temperature, 600 °C for instance, in argon environment. The Fe-based component was then removed by hydrochloric acid resulting in a sample that had thin planar/lamellar structure with short and disordered graphite-like layer. It is believed that the addition of $FeCl_3$ is conducive to the oxidation and polymerization of the monomers, as well as beneficial for the graphitization and porosity formation of the derived carbon.

In the absence of bulk substrates and any other host, DOPA rapidly self-polymerize into PDA nanoparticles using Tris as the buffering agent.[53] The size of the nanoparticles is around 100 nm. Upon carbonization at 800 °C in N_2 or Ar, the PDA nanoparticles are converted to carbon nanoparticles. Possible cracking of the particles can be avoided by slowing down the heating rate. The choice of solvent and buffering agent plays a crucial role in improving the spherical shape of the C-PDA nanoparticles. In our previous work we found that by controlling the polymerization rate using H_2O/ethanol mixed solvent, PDA nanoparticles with very fine spherical shape can be obtained.[64] In 2013, K. Ai et al. proposed another straightforward solution method to obtain monodispersed and size-controlled carbon sub-micrometer spheres at a large scale.[59] In their work, dopamine hydrochloride aqueous solution was injected into the mixture of ammonia, ethanol, and deionized water (DI H_2O) to allow for immediate self-polymerization. After reaction for 30 hrs, the final product was obtained by centrifugation, washing, drying, and carbonization in Ar at 800 °C. Perfect spheres with varying size, which was strictly controlled by the ratio of ammonia to DOPA, from 120 nm to 780 nm were obtained, as shown typically in Fig. 5a. Hollow carbon spheres with particle size of approximately 400 nm were prepared separately by Dai et al. and Chen et al. in 2011 through coating DOPA onto silica spherical template followed by carbonization and HF etching.[54, 55] The structural integrity and spherical morphology was perfectly maintained after removing the template, while the wall thickness varied from a few nanometers to tens of nanometers in accordance with different coating conditions (Fig. 5b). Using nano-$CaCO_3$ (40-110 nm in size) as the template, nitrogen-doped porous carbon was obtained through PDA coating followed by carbonization and removal of $CaCO_3$ in HCl solution.[65] In 2013, Wu et al. prepared well-ordered nitrogen-doped nanoporous carbon via PDA in-situ coating on silica template followed by carbonization and removal of the template.[66] In 2014, Ahmed et al. prepared nitrogen- and boron-co-doped core-shell carbon nanoparticles,[67] which was achieved using carbon particles as the core, PDA as the nitrogen precursor, and 3-aminophenylboronic acid (ABA) as the boron precursor. The carbon particles were covered by PDA followed by ABA thin layer. The annealing at 900 °C in N_2 atmosphere led to nitrogen- and boron-co-doped carbon nanoparticles.

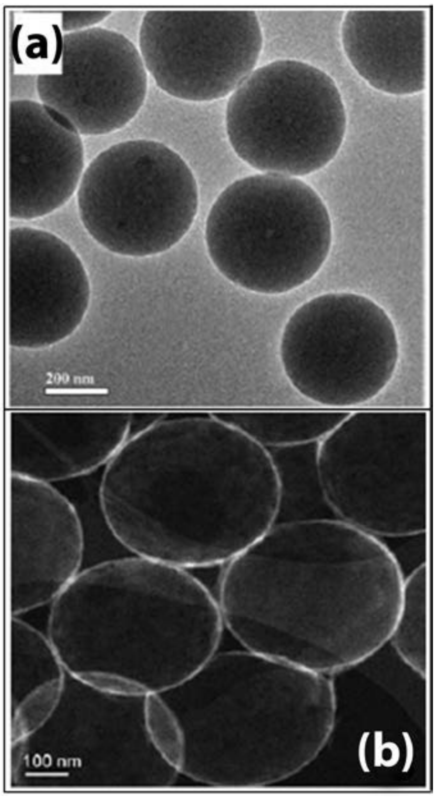

Fig. 5 Typical morphologies of C-PDA (a) solid nanospheres with average diameter of 380 nm [reprinted with permission from ref. [59]. Copyright 2012, John Wiley and Sons], and (b) hollow nanospheres [reprinted with permission from ref. [54]. Copyright 2011, John Wiley and Sons].

Carbon dots were also obtained via a facile and green one-step hydrothermal route using dopamine as the source.[62] Without the use of any buffering agent, the aqueous

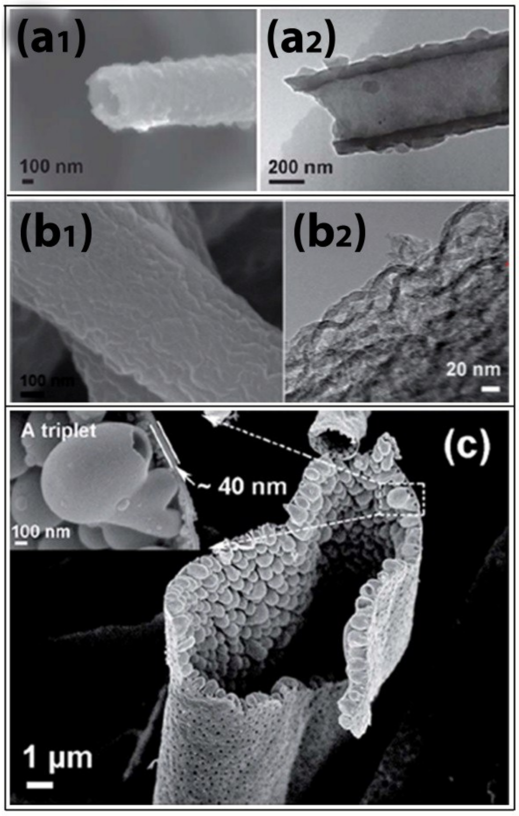

Fig. 6 The morphologies of C-PDA (a_1 and a_2) nanotubes [reproduced from Ref. [61] with permission from The Royal Society of Chemistry], (b_1 and b_2) porous nanofibers [reproduced from Ref. [68] with permission from The Royal Society of Chemistry] and (c) nanocups-on-microtubes [reproduced from Ref. [69] with permission from The Royal Society of Chemistry].

dopamine solution was heated up to 180 °C in a sealed Teflon-lined autoclave and kept at 180 °C for 6 hrs. The sample was then collected after dialysis and centrifugation. The size of the carbon dots ranges from 3 to 5 nm. It is claimed that the formation of carbon dots experiences the following process: firstly the graphitization of dopamine that forms core, and secondly the in-situ coating of polymerized dopamine onto the core and further carbonization into carbon.

One dimensional (1D) C-PDA nanostructures, including hollow nanofibers, mesoporous nanofibers, and nanocups attached on microtubes (nanocups-on-microtubes), were prepared by our group. These 1D C-PDA nanostructures were obtained by PDA coating onto various 1D templates, which can be removed in the subsequent step. For preparation of C-PDA hollow nanofiber, PDA was firstly coated onto a loose lump of electrospun polyacrylonitrile (PAN) nanofibers suspended in DOPA aqueous solution (0.3 mg/mL) using Tris as buffering agent. The PAN core was then dissolved in the N, N-dimethylformamide (DMF), leaving PDA shells in 1D geometry without affecting their structural integrity. The PDA nanotubes were finally carbonized into C-PDA nanotubes as shown in Fig. 6a. The diameter and wall thickness of the nanotubes is around 560 nm and 40 nm, respectively. For C-PDA porous nanofibers and nanocups-on-microtubes, electrospun PS nanofibers with interpenetrated nanochannels and surface-located pores, respectively, were used as templates. Coating PDA on the above two templates followed by annealing in inert gas led to C-PDA porous nanofibers and nanocups-on-microfibers (Fig. 6b_1, b_2 and c).[68, 69] Interpenetrated pores were formed in the C-PDA porous nanofibers, and the surface of the nanofibers may have open pores or may be wrapped by a continuous shell, depending on the PDA coating thickness. In the nanocups-on-microtubes, a large number of ellipsoid-shaped nanocups are firmly attached on the C-PDA microtubes.

4. Integration of inorganic nanostructures with polydopamine-derived carbon

4.1 Direct coating of PDA on inorganic nanostructures

Thanks to the ability of DOPA to self-polymerize in basic aqueous solutions in ambient conditions and its versatile adhesive properties, PDA can be directly coated onto numerous kinds of inorganic nanostructures with adjustable thickness via in-situ route. This leads to a facile approach to novel composite nanostructures for a wide range of applications. For example, C-PDA coating has been demonstrated as a very useful approach to improve the electrical conductivity of metal oxide nanoparticles for electrochemical and some other applications. In 2012, Kong et al. reported controlled coating of PDA on hydrothermally obtained SnO_2 nanoparticles to produce bridged C-PDA-coated SnO_2 nanoclusters.[28] As shown in Fig. 7a_1 and a_2, the SnO_2 nanoparticle clusters, which have the size of about 50 nm with some mesopores in between, are uniformly covered by a

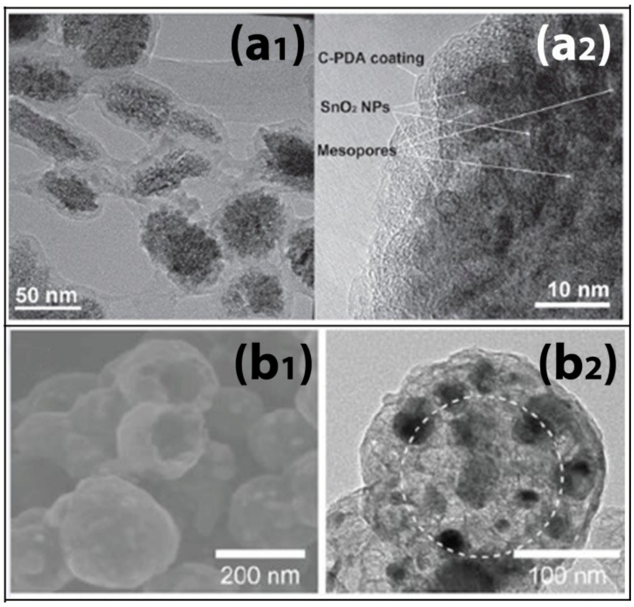

Fig. 7 Morphologies of (a_1 and a_2) C-PDA/SnO_2 nanoclusters prepared from PDA coating and carbonization [reproduced from Ref. [28] with permission from The Royal Society of Chemistry], and (b_1 and b_2) mesoporous hollow carbon microspheres embedded with Fe_3O_4 nanoparticles [reprinted with permission from Ref. [70]. Copyright (2014), American Chemical Society].

C-PDA thin layer with thickness of around 5 nm. The deposition of PDA layer onto other metal oxides via in-situ coating followed by carbonization was also carried out to improve the electrical conduction of the oxide nanostructures as well as protect the desired morphology from collapsing in the case of volume change during electrochemical process. C. Li et al. designed a novel one-dimensional highly graphitic carbon-tipped manganese oxide/mesoporous carbon/manganese oxide hybrid nanowire.[71] It was fabricated by multiple steps including coating PDA onto MnO_2 nanowires in the presence of a structure-directing agent (a PEO-PPO-PEO copolymer (P123)), mixing the coated nanowires with $Mn(NO_3)_2 \cdot 4H_2O$ in isopropanol followed by refluxing, and annealing at 850 °C in argon flow. As a result, a thin disordered mesoporous carbon layer was coated onto the MnO_2 nanowires with graphitic carbon observed on the tip region, while crystalline MnO_2 nanoparticles were distributed on the carbon layer as well. Other than the aforementioned work, DOPA was also polymerized on TiO_2 microspheres/nanospheres,[58, 72] $ZnSnO_3$ nanocubes,[73] Fe_2O_3/SnO_2 hybrid nanofibers,[74] $ZnFe_2O_4$ nanorods,[75] $Li_3V_2(PO_4)_3$ particles,[76] and silica nanoparticles via similar routes to create C-PDA coating by carbonization.[77] The C-PDA-coated TiO_2 microspheres could be further converted to C-PDA-coated $Li_4Ti_5O_{12}$ microspheres via hydrothermal treatment in the presence of LiOH. It is worth noting that PDA can also be coated onto metal oxide nanostructures by in-situ polymerization of DOPA without using Tris as buffer. For Example, J. Lee et al. reported that a C-PDA layer with thickness of only 2-3 nm could be formed on $LiFePO_4$ nanocrystals through aqueous polymerization route without the use of buffering agent.[78]

Another class of C-PDA-based hybrid nanostructures that are worth mentioning is magnetic mesoporous carbon, which has found wide use in chemical removal and proteomic area. Magnetic carbon is basically a composite with magnetic Fe_3O_4 embedded in C-PDA; therefore, it can be easily separated from solutions or other solid mixtures by magnets. A few such systems have been reported. G. Cheng et al. simply deposited PDA layer onto Fe_3O_4 microspheres and carbonized them to get mesoporous hollow carbon microspheres embedded with Fe_3O_4 nanoparticles.[70] After the deposition and carbonization, the Fe_3O_4 microspheres de-aggregate into small nanoparticles, leaving pores inside the carbon nanospheres and small Fe_3O_4 nanoparticles that attached onto the inner surface of carbon (Fig. 7b_1 and b_2). S. Wang et al. deposited C-PDA layer onto Fe_3O_4@$CaCO_3$ nanocomposite and then removed the $CaCO_3$ by acid, forming Fe_3O_4 nanoparticles fully embedded in C-PDA layer,[79] which were mesoporous and interconnected to one other. S. Liu et al. obtained flowerlike magnetic mesoporous carbon through multiple steps,[80] including silica layer deposition onto Fe_3O_4 nanospheres, Mg-Al LDH formation on surface of Fe_3O_4@SiO_2, C-PDA coating onto Fe_3O_4@SiO_2@Mg-Al LDH, and acid etching to remove LDH framework. Flowerlike carbon shell with average mesopores of 3.8 nm was finally formed and grafted perpendicularly onto the surface of Fe_3O_4@SiO_2 nanospheres. Recently, another method using Fe(III)-dopamine complexation-assisted one-pot synthesis was presented to obtain Fe_3O_4/N/C hollow nanospheres using PDA as carbon source,[82] which will be elaborated in section 4.3 of this review.

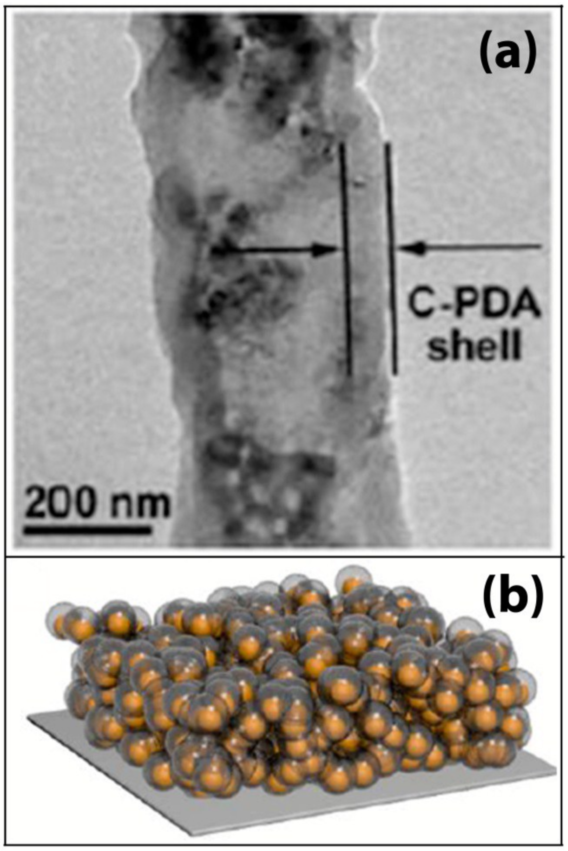

Fig. 8 (a) Morphology of Si nanoparticles encapsulated in hollow C-PDA nanofibers [reproduced from Ref. [61] with permission from The Royal Society of Chemistry], (b) a schematic demonstration of framework of Si/C-PDA yolk-shell nanostructures. Both are obtained through PDA coating, etching and carbonization [reprinted with permission from ref. [81]. Copyright (2012) American Chemical Society].

As presented in section 3.2, C-PDA hollow nanostructures could be facilely prepared via coating PDA onto templates, e.g., nanofibers, nanospheres, etc., followed by etching and/or carbonization. Such hollow carbon nanostructures can be used to host inorganic components to create various hybrid nanostructures. For example, silicon (Si) is considered as one of the most active anode compounds in rechargeable lithium ion batteries (LIBs) due to its extremely high theoretical capacity (> 4000 mA h g^{-1}) and relatively low and stable discharge/charge potential stage. Nevertheless, the ~ 400 % volume expansion during lithiation/de-lithiation, as well as its poor electrical conductivity, remains the main obstacle to good performance. To address such issues, Kong et al. encapsulated Si nanoparticles in C-PDA hollow nanofibers, the morphology of which is shown in Fig. 8a, via electrospinning of polyacrylonitrile (PAN)/Si solution followed by PDA coating, etching in DMF, and carbonization at 700 °C.[61] After carbonization, the diameter of the hollow nanofibers is about 440 nm, and the thickness of the C-PDA shell is only 40 nm. Si nanoparticles are well encapsulated in the hollow nanofibers.

The C-PDA/Si hybrids with other structures were also reported by other groups. Y. Cui et al. prepared a special Si-based yolk-shell structure via depositing PDA layer onto Si/SiO_2 core/shell nanospheres followed by carbonization and HF treatment. The HF treatment etches SiO_2, leading to Si yolk-carbon shell nanocomposites with void in between.[81] The carbon shell with thickness of 5-10 nm is interconnected and forms a self-supporting framework (Fig. 8b). As a similar work, D. Wang et al. also applied C-PDA coating onto Si/SiO_2 core/shell nanospheres via in-situ polymerization and removed SiO_2 layer by HF etching.[83] The volume ratio of void/Si, which is dependent on the thickness of SiO_2 shell, can be adjusted to produce appropriate voids that are useful for accommodating the volume expansion of Si during electrochemical procedure. This yolk-shell nanostructure can also be formed with other components, such as iron oxide@carbon yolk-shell nanostructure and Au@C yolk-shell monodisperse spherical nanocomposites,[54, 84] using similar route, i.e., silica coating followed by PDA coating, carbonization, and silica etching. It is also reported that paramecium-shaped α-MnO_2 hierarchical hollow structure was prepared with the assistance of PDA coating by Che's group.[85] In this case, Fe_2O_3 spindle-like templates were used to prepare hollow C-PDA shells first, and flaky crystals of MnO_2 were then hydrothermally grown on the hollow shells.

4.2 Post-introduction of inorganic components into C-PDA nanostructures

An alternative to the route of PDA coating followed by carbonization is to introduce inorganic components into/onto PDA hosts followed by carbonization. For example, mixture of Fe and Fe_3C could be incorporated into C-PDA sub-micron spheres via adding iron (II) acetate ($Fe(CH_3COO)_2$) into a water suspension containing the PDA spheres followed by centrifugation and heat treatment at 800 °C.[59] Spherical morphology is maintained after centrifugation, and Fe^{2+} is absorbed by the PDA spheres through interactions with catechol and N-H groups. After carbonization, both micropores and mesopores are introduced into the spheres while the salts are converted to Fe@Fe_3C particles that are embedded in the graphitized C-PDA matrix. The abilities of PDA to adsorb transitional metal ions and reduce some noble metal ions, such as Ag^+,[40] Pt^{3+}, Au^{3+}, also enabled surface decoration of inorganic nanostructures on the C-PDA coatings. For instance, Ag nanoparticles were used to decorate PDA-coated ZnO nanorod arrays to introduce efficient plasmonic effect that is beneficial to the photoelectrochemical process.[86] Firstly, the PDA layer was deposited onto ZnO nanorod arrays via normal solution route to produce PDA-coated ZnO nanorod arrays, which were then immersed into silver nitrite ($AgNO_3$) aqueous solution to reduce Ag^+ to Ag by PDA layer in order to attach it onto the layer surface. Carbonization was finally applied to convert PDA layer to a highly graphitized C-PDA layer with intact Ag nanoparticle attachment covered by a thin C-PDA layer, forming C-PDA-coated ZnO nanorod arrays with decoration of Ag nanoparticles (Fig. 9a and b). Using similar adsorption followed by reduction-cum-carbonization approaches, Pt nanoparticles were also introduced onto PDA-coated silica, PDA-coated carbon nanotubes, PDA-coated carbon nanospheres, and PDA-coated carbon black via injection of Pt precursors,[77, 87] and gold nanoparticles were attached onto the surface of C-PDA hollow nanospheres.[88]

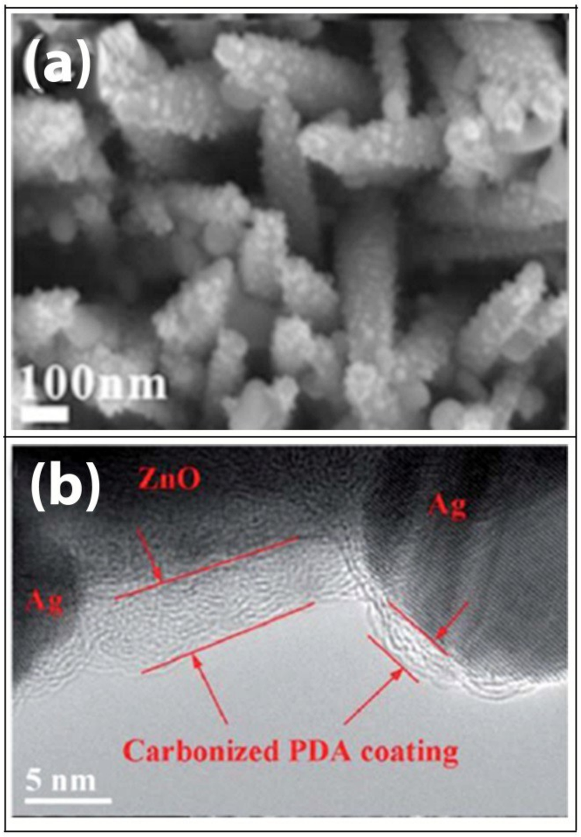

Fig. 9 (a) SEM image of PDA-assisted Ag nanoparticles-decorated ZnO nanorod arrays, (b) the HRTEM image showing the anchoring of Ag nanoparticles onto ZnO surface by C-PDA layer [reproduced from Ref. [86] with permission from The Royal Society of Chemistry].

Another interesting route is that hollow/porous C-PDA nanostructures could also act as nano-reactors for synthesis of inorganic nanostructures. Our group recently introduced MoS_2 nanosheets into C-PDA nanocups-on-microtubes.[69] By vertically immersing the free-standing mat of nanocups-on-microtubes into aqueous solution of sodium molybdate dehydrate ($Na_2MoO_4 \cdot 2H_2O$) and thioacetamide (TAA), the precursors were trapped in the nanocups. Hydrothermal growth of MoS_2 nanosheets then occurs inside the nanocups through putting the filled nanocups-on-microtubes in an autoclave. Randomly oriented MoS_2 nanosheets are formed in the nanocups, while the C-PDA morphology remains intact due to the strong mechanical strength (Fig. 10a_1 and a_2). Similarly, via a solution route using $ZnSO_4 \cdot 7H_2O$ and $FeSO_4 \cdot 7H_2O$ as precursors, zinc iron oxide ($ZnFe_2O_4$) nanoneedles were grown on the surface and inside the nanochannels of C-PDA mesoporous nanofibers (Fig. 10b_1~b_4).[68] The free-standing

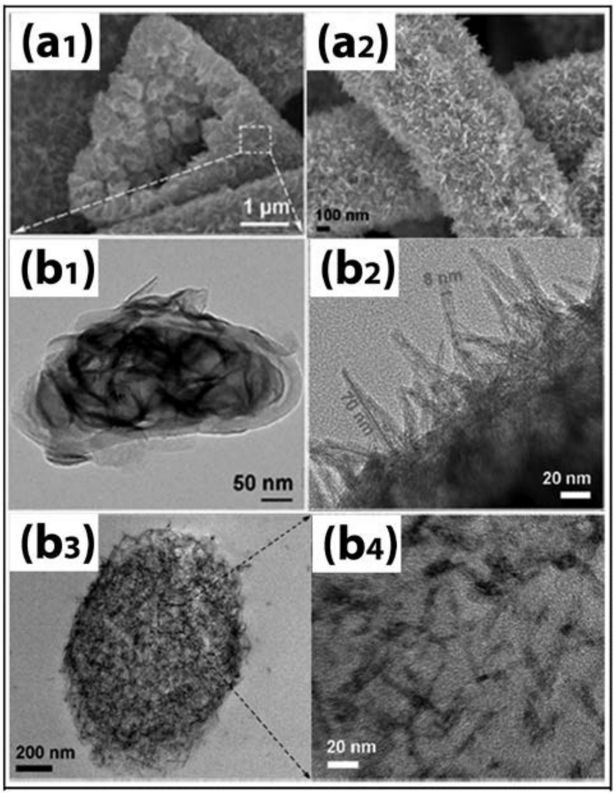

Fig. 10 (a_1 and a_2) Morphologies of MoS_2 nanosheets grown within C-PDA nanocups [reproduced from Ref. [69] with permission from The Royal Society of Chemistry]. (b_1) SEM images of $ZnFe_2O_4$ nanoneedles grown on C-PDA porous nanofibers, (b_2) the surface region and (b_3 and b_4) cross-sectional views of $ZnFe_2O_4$ nanoneedles-on-C-PDA porous nanofibers [reproduced from Ref. [68] with permission from The Royal Society of Chemistry].

mesoporous nanofibrous mat was soaked in $ZnSO_4{\cdot}7H_2O$/ $FeSO_4{\cdot}7H_2O$ solution for certain time to absorb precursors and then suspended above the concentrated ammonium hydroxide to convert the precursors into zinc complexes with hydroxide or ammonia and $Fe(OH)_3$. Finally, the intermediates were annealed to form $ZnFe_2O_4$ nanoneedles.

4.3 Transitional metal-mediated polymerization of dopamine for in-situ formation of composite nanostructures

Transitional metal-mediated polymerization of DOPA is an attractive one-pot approach for the synthesis of C-PDA/inorganic composite nanostructures. The complexation between catechol groups and transitional metal species has been widely studied. So far DOPA has been reported to be able to form complexes with metal species containing Fe(III), Ni(II), Co(II), Zn(II), Mn(II), Ca(II), and Ti(II).[44-49, 89-92] Thus, when transition metal species are present in DOPA polymerization systems, complexation of DOPA with transition metal species and covalent polymerization of DOPA may occur simultaneously, resulting in hybrid nanostructures with uniformly embedded transition metal species, which can be converted to C-PDA/metal or metal oxide composite nanostructures by carbonization.

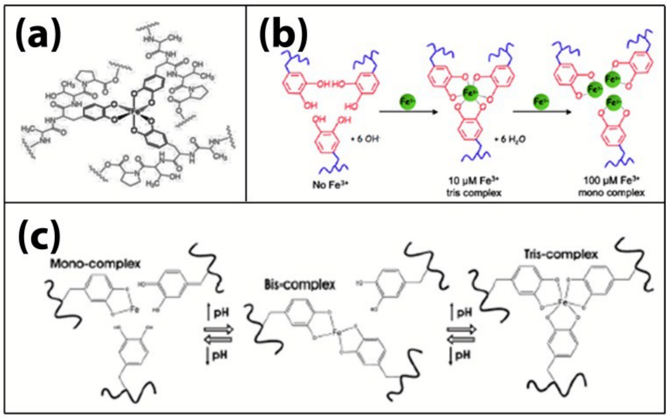

Fig. 11 (a) Proposed mussel adhesive metal-protein cross-link [reprinted with permission from ref. [46]. Copyright 2003, John Wiley and Sons], (b) multiple bidentate complexation of Fe^{3+} by DOPA ligands at different Fe^{3+} concentrations [reprinted with permission from ref. [91]. Copyright (2010) National Academy of Sciences, USA], (c) the pH-dependent stoichiometry of Fe^{3+}-catechol complexes [reprinted with permission from ref. [48]. Copyright (2011) National Academy of Sciences, USA].

The complexes of Fe(III) ions with DOPA are the most intensively studied systems. In 2004, J. Wilker et al. proposed that each Fe(III) ion in the mussel plaques cross-links three DOPA units, forming $[Fe(DOPA)_3]$ structure (Fig. 11a).[46] Such complexation improves the hardness and extensibility of the matrix.[89, 90, 93, 94] In 2010, Waite et al. found that the bridging effect of Fe^{3+} in DOPA is reversible in water and concentration dependent.[91] At low Fe^{3+} concentration of 10 µM, tris-complex forms; whereas, when the concentration increases to 100 µM, the tris-complex collapses into monocatecholato-iron structure (Fig. 11b). In the following year, the same group further studied the effect of pH on the catechol-Fe^{3+} interpolymer cross-linking,[48] and verified that the complexation between Fe^{3+} and catechol groups is pH-controlled. At acidic environments with pH < 5.6, the complex is mono-specie, i.e., [Fe(DOPA)]; whereas, when the pH falls between 5.6 and 9.1, a bi-complex with $[Fe(DOPA)_2]$ structure forms; lastly, at base environments with pH > 9.1, the complex is re-structured into tris-one (Fig. 11c).

The ability of Fe(III) ions to form complexes with DOPA provided a facile one-pot route to introduce Fe species into C-PDA matrix. For instance, to create an efficient ORR catalyst, PDA layer was coated onto silica nanospherical template in the presence of $FeCl_3$, resulting in a hybrid shell composted of complex of PDOPA and Fe(III) species. After carbonization at 750 °C and subsequent etching out silica in KOH (3.0 M), hollow composite nanospheres composed of highly graphitized C-PDA (about 120 nm in diameter) embedded with well-dispersed Fe_3O_4 nanoparticles were obtained (Fig. 12a_1 and a_2).[82] The wall thickness, Fe loading, and nanoparticles size could be well controlled, resulting in optimized composite hollow nanospheres with 10 nm for wall thickness, 10.6 at% for Fe atomic content and 9 nm for Fe_3O_4 nanoparticle size, which possesses large specific surface of 736 m^2 g^{-1} and pore size of mainly 2 – 9 nm.

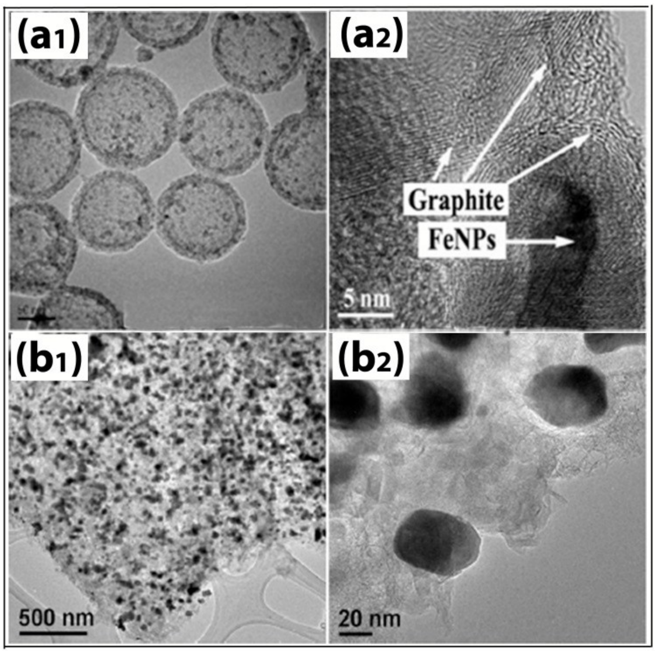

Fig. 12 Morphologies of (a_1 and a_2) highly graphitized C-PDA hollow nanospheres embedded with well-dispersed Fe_3O_4 nanoparticles [reproduced from Ref. [82] with permission from The Royal Society of Chemistry] and (b_1 and b_2) Ni@C-PDA hybrids [reprinted with permission from ref. [43]. Copyright 2014, John Wiley and Sons].

Although some transition metal ions do not form complex with DOPA, the polymerization of DOPA may still be mediated by the addition of transitional metal species.[43] For example,the kinetics for the formation of solid DOPA “polymerization” products is significantly affected by the addition of transition metal species. It was found that Ni(II) species does not form complex with DOPA monomer and its presence in DOPA polymerization system does not affect the polymerization rate in the first few hours, whereas it later accelerates the rate of the formation of solid polymerization product. This indicates that Ni(II) species may interact with DOPA oligomers rather than monomers, forming Ni(II)-PDA complex. Normally, the one-pot synthesis process is carried out by adding metal salts into DOPA aqueous solution with controlled molar ratio of metal ions to DOPA followed by adding Tris buffer to trigger the polymerization. The results reported by Yang et. al show that transition metal species, such as Ni(II), Co(II), and Mn(II) species, could indeed be incorporated into the formed PDA in quantity via this facile one-pot route. The hybrids could be in the form of powders or be coated on organic or inorganic nanostructures, for instance, graphene. The metal species are distributed homogeneously in the PDA matrix. After carbonization at 800 °C, heterogeneous nanostructure forms. A large number of metal or metal oxide nanoparticles, for example, metallic Ni, Co and MnO, are uniformly embedded in the highly graphitized porous carbon (Fig. 12b_1 and b_2). These composite nanostructures could be used in various areas, such as catalysis and energy storage.

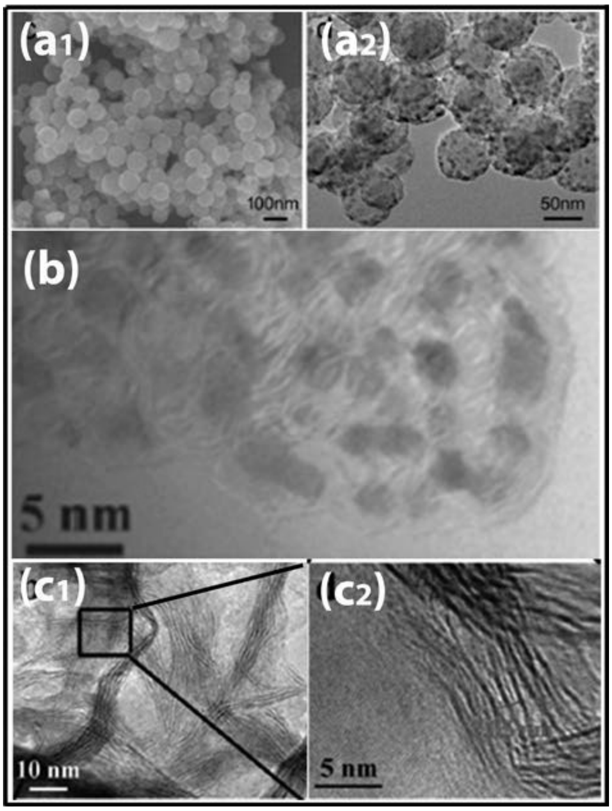

Fig. 13 (a_1 and a_2) Morphologies of $ZnFe_2O_4$@C-PDA nanospheres [reproduced from Ref. [95] with permission from The Royal Society of Chemistry]. (b) TEM image of DOPA-Mo(VI) complex, (c_1 and c_2) morphologies of crumpled MoS_2 nanoplates with C-PDA layer sandwiched in between [reproduced from Ref.[96] with permission from The Royal Society of Chemistry].

The one-pot approach has also been applied to introduce binary metal oxide nanoparticles into C-PDA. For example, for the electrochemical application as anode of LIBs, binary metal alloy nanoparticles, zinc ferrite ($ZnFe_2O_4$), were introduced into C-PDA nanospheres using zinc chloride ($ZnCl_2$) and iron chloride tetrahydrate ($FeCl_2{\cdot}4H_2O$) as precursors.[95] It was shown that Zn^{2+}, unlike Fe^{2+}, does not form complex with DOPA but instead forms Zinc hydroxide, which may interact with the amine ligands. Therefore, both Zn^{2+} and Fe^{2+} are successfully incorporated into PDA during the polymerization. The annealing at 600 °C in argon converts Zn- and Fe-based species into $ZnFe_2O_4$ nanoparticles. The nanoparticles are well distributed and embedded in the graphitic C-PDA nanospheres (Fig. 13a_1 and a_2). Single-layer MoS_2-carbon nanocomposites were also prepared with the assistance of DOPA-Mo(VI) complexation.[96] By simply mixing DOPA and sodium molybdate (Na_2MoO_4), DOPA-Mo(VI) complex forms, which exhibits sea-island morphology with evenly distributed Mo-rich islands in the sea of a wrinkled layer structure composed of DOPA oligomers (Fig. 13b). The following hydrothermal treatment in the presence of thioacetamide (TAA) at 200 °C produces MoS_2 and partially carbonizes PDA. Further annealing at 700 °C in argon environment leads to crumpled MoS_2 nanoplates containing 3-5 disordered MoS_2 layers with carbon layer sandwiched in between, due to the maintaining of the pre-formed DOPA-Mo(VI) complex after the treatment (Fig. 13c_1 and c_2).

Besides the complexation-based in-situ route, the reduction capability of catechol moiety on noble metal ions, such as Au^{3+} and Ag^+, offers another in-situ way to form nanocomposites that show promising catalytic properties. It has been reported that in the presence of Ag^+, the catechol groups oxidize through reducing Ag^+ into metallic Ag, and then polymerize with amines to form PDA.[41] Similarly, simultaneous reduction of $HAuCl_4$ and polymerization of DOPA occurs when $HAuCl_4$ is added into DOPA alkaline solution (pH = 9), forming Au/PDA nanoparticles.[42] After carbonization at 500 °C in argon, Au/C-PDA composites with Au nanoparticles embedded in C-PDA particles were obtained.

5. Applications of (C-PDA) and C-PDA-based composite nanostructures

5.1 Applications in energy storage and harvest

a) As anodes of lithium-ion batteries (LIBs). To date, graphite is the only major commercial anode material for LIBs. It has been reported that lithium ions are intercalated into graphite through staging phenomenon, i.e., the formation of LiC_6 intercalates (Stage I), which has the most significant contribution to lithium ion storage, is accompanied by the occurrence of stage II (forming LiC_{12}), stage III (forming LiC_{18}), and stage IV reactions.[97-100] For partially graphitized carbon, the crystallinity, porosity, doping of heteroatoms (N, B, etc.) as well as the surface functional groups play crucial roles in determining the lithium intercalation mechanism and the electrochemical performance.[101] Indeed, C-PDA nanostructures are found to be capable of alloying with lithium ions through different mechanisms. The substantial amount of pyridinic and pyrrolic N in C-PDA as well as the N-doping-induced structural disorder and defects enhance its capability of alloying/de-alloying with lithium ions. As a result, the lithiation/de-lithiation behavior of C-PDA is mainly metallic lithium plating,[102-104] rather than the standard stage I alloying/de-alloying processes that normally occur in graphite. C-PDA hollow nanofibers, mesoporous nanofibers, and nanocups-on-microtubes have been explored as LIB anode materials. The reversible capacities of C-PDA hollow nanofibers, mesoporous nanofibers, and nanocups-on-microtubes at current rate of 100 mA g^{-1} are around 440, 480, and 550 mA h g^{-1}, respectively,[61, 68, 69] which are higher than the theoretical capacity of graphite, 372 mA h g^{-1}. Since these C-PDA nanostructures have similar microstructures (like that of N-doped multilayer graphite), their different specific surface areas caused by their different morphologies should be the major reason for the variation in capacity.

C-PDA-based nanocomposites with varied structures/morphologies can be prepared through different routes, as discussed in the previous section, and are promising anode candidates for LIBs. In these nanocomposites, the C-PDA thin coatings on various anode materials can act as electrically conductive protection layers. They buffer the volume change of the anode materials during lithiation/de-lithiation, conduct charges, as well as ensure structural stability. As an example, the interconnected C-PDA-coated SnO_2 nanoclusters with SnO_2 content of around 80 wt% could deliver stable reversible capacity of about 700 mA h g^{-1} at current rate of 100 mA g^{-1}, realizing as high as 98 % of the theoretical capacity of the hybrid.[28] This is much higher than that of pristine SnO_2 nanoparticles without the C-PDA coating. Other than enhancing charge transport and buffering the volume change, the C-PDA coating on SnO_2 nanoparticles also prevents the re-aggregation of SnO_2 nanoparticles during lithiation/de-lithiation, improving cycle life of the anode. Other reported C-PDA-based nanocomposite LIB anode systems include C-PDA-coated microspheres of $Li_4Ti_5O_{12}$ aggregates,[58] C-PDA-coated TiO_2 nanospheres,[72] $ZnSnO_3$ nanocubes,[73] C-PDA-coated Fe_3O_4/SnO_2 hybrid nanofibers,[74] and C-PDA-coated $ZnFe_2O_4$ nanorods.[75] In most cases of direct coating on inorganic nanostructures, the contact between C-PDA layer and active materials is fairly compact, and a coating thickness of around 10 nm or less is adequate for effectively protecting the anode materials and at the same time ensuring good charge conduction.

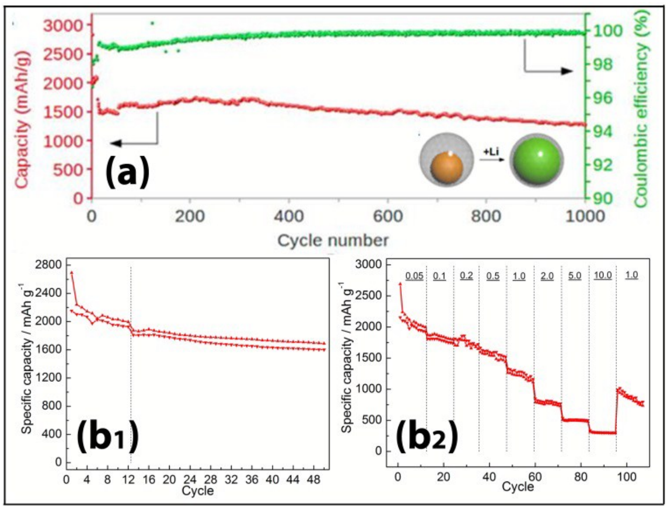

Fig. 14 (a) Cycling performance of interconnected Si/carbon yolk/shell nanocomposites [reprinted with permission from ref. 81. Copyright (2012) American Chemical Society]. (b_1) Cycling and (b_2) rate performance of Si nanoparticles encapsulated in C-PDA hollow nanofibers [reproduced from Ref. 61 with permission from The Royal Society of Chemistry].

In comparison with the direct coating method, the post-introduction of electrochemically active materials into C-PDA matrix and the etching approach (forming yolk-shell structure) give rise to weaker interactions between the two components. When C-PDA nanostructures are used as host/support to facilitate the in-situ formation of active components, voids/pores are normally formed at interfaces. Compared to the compact interface provided by the direct coating method, these interfacial voids/pores offer much reduced resistance to the diffusion of electrolyte and lithium ions, as well as extra spaces for accommodating the volume expansion of the active components. To demonstrate these functions, a few examples are elaborated below. Y. Cui et al. reported that with Si content of about 71 wt%, the interconnected Si/C-PDA yolk/shell nanocomposites could deliver a stable capacity of about 1500 mA h g^{-1} at current rate of 1C (Fig. 14a) with capacity retention of 74 % after 1000 cycles.[81] It was also claimed that with void/Si volume ratio of about 3, the nanocomposites could achieve the best electrochemical performance due to the most effective accommodation as illustrated schematically in inset of Fig. 14a.[83] Kong et al. encapsulated Si nanoparticles with average size of around 50 nm in C-PDA hollow nanofibers and studied the electrochemical performance of the hybrids as LIB anodes.[61] With Si content of 47.9 wt%, reversible capacity of about 1600 mA h g^{-1} at 100 mA g^{-1} was achieved, and the capacity remained as high as 500 and 300 mA h g^{-1}, respectively, at 5 and 10 A g^{-1} (Fig. 14b_1 and b_2). The reversible capacity is about 72.6 % of the theoretical capacity of the hybrid. During discharge/charge processes, the hollow nature of the C-PDA nanofibers ensures enough space for lithium insertion and electrolyte transport. Furthermore, the C-PDA functions as charge conductor and electrochemically active phase that contributes to the overall performance. Similar functions of C-PDA also helped to boost the performance of other C-PDA-based nanocomposite anodes, despite that the contact between the active component and C-PDA may vary owing to their different preparation routes. For instance, MoS_2 nanosheets were hydrothermally synthesized in C-PDA nanocups.[69] Considering the MoS_2 content of 46 wt%, the normalized capacity of MoS_2 nanosheets in such nanostructure is as high as 1524 mA h g^{-1}, indicating high utilization of activity of MoS_2 with possible extra lithium adsorption at the interfaces of C-S-Mo. Recently, the growth of $ZnFe_2O_4$ nanoneedles on the outer and inner surface of the C-PDA mesoporous nanofibers was also reported.[68] The $ZnFe_2O_4$ activity is also highly utilized, indicating its significant contribution to the overall capacity of the anode.

The one-pot construction of C-PDA/metal (or metal oxide) hybrid nanostructures through complexation, as discussed in Section 4.3, is a more facile route to prepare C-PDA-based nanocomposite anodes. For example, the complexation of DOPA and Mo^{VI} followed by hydrothermal treatment leads to single-layer MoS_2-N-doped carbon sandwich-like nanocomposites. With MoS_2 content of 76 wt%, the nanocomposites possess a stable capacity of 500 mA h g^{-1} for more than 800 cycles at 1.0 A g^{-1}.[96] Resulting from complexation/interaction of DOPA with Fe and Zn species, $ZnFe_2O_4$ nanoparticles were introduced into C-PDA nanospheres.[95] The nanocomposites deliver stable capacity of 914/895 mA h g^{-1} at current rate of 0.1 A g^{-1}, and 409/323 mA h g^{-1} at 5.0/10.0 A g^{-1}, respectively. The one-pot route is simpler than other routes for incorporation of active inorganic components into C-PDA. The incorporated components can be more uniformly distributed in the C-PDA matrix for enlarging the contact area and enhancing the protection function. Nevertheless, the complexation is restricted to certain species, and the composition is determined by the coordination chemistry rather than the feed ratio. Clarification of the complexation mechanisms is necessary to fully utilize the potential of this simple approach.

b) As cathodes of lithium-ion batteries. Thin C-PDA layers could also be created on LIB cathode materials, such as $LiFePO_4$ nanocrystals and $Li_3V_2(PO_4)_3$ nanoparticles. Similar to that in anodes, the C-PDA functions as structural stabilizing layer as well as charge conductor. As a cathode, the C-PDA-coated $LiFePO_4$ nanocrystals exhibit high rate capacity with excellent cyclability (143 mA h g^{-1} at current density of 1.7 A g^{-1}).[78] The C-PDA-coated $Li_3V_2(PO_4)_3$ nanoparticles with coating thickness of 7 nm deliver specific capacity of 109 mA h g^{-1} at current density of 1 C with capacity loss of only 4.6 % after 100 cycles, as well as high rate capacity of 74 mA h g^{-1} at high current density of 10 C.

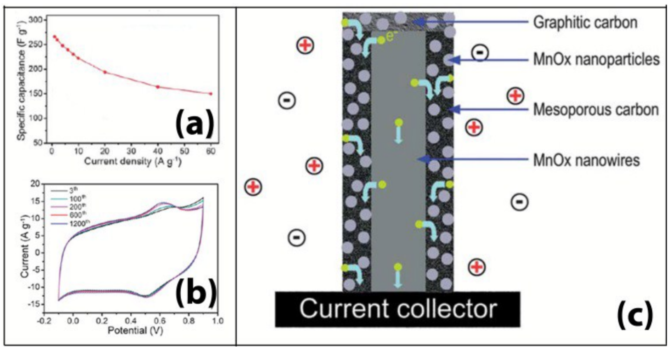

Fig. 15 (a) Rate performance and (b) cyclability of graphitic carbon-tipped manganese oxide/mesoporous carbon/manganese oxide hybrid nanowires. (c) The schematic illustration of the nanohybrid, showing the functions of each segment [reproduced from Ref. [71] with permission from The Royal Society of Chemistry].

c) As electrodes of supercapacitors. Another popular energy storage devices are supercapacitors. The most significant advantages of such devices are super-fast charge/discharge speed and excellent cyclability. So far, many materials have been attempted as electrode of supercapacitors,[105-107] and C-PDA, which has been intensively investigated, is one of them. Well-ordered N-doped nanoporous C-PDA framework was prepared using DOPA as the starting material and used as supercapacitor electrodes.[66] The framework exhibits high capacitance (538 F g^{-1} and 358 F g^{-1} at sweep rates of 5 mV s^{-1} and 50 mV s^{-1}, respectively) and good cycling stability (93 % capacitance retention at 3 A g^{-1} after 5000 cycles). In addition to the large surface area of the framework that offers abundant reaction sites, the doping of appropriate nitrogen functional groups significantly improves the electrochemical capacitive behaviour by providing huge pseudocapacitance via pseudo-capacitive redox reactions.

C-PDA-based nanocomposites have also been studied as electrodes of supercapacitors. In these systems, C-PDA acts as both charge conductor and capacitance contributor. C. Li et al. prepared graphitic carbon-tipped manganese oxide/mesoporous carbon/manganese oxide hybrid nanowires and studied their electrochemical property as electrode of supercapacitors.[71] The hybrid nanowires with optimized carbon layer deliver specific capacitance of 226 F g^{-1} at a scan rate of 10 mV s^{-1} and 266 F g^{-1} at a current density of 1 A g^{-1}. The capacitance is still as high as 150 F g^{-1} at a higher current density of 60 A g^{-1} (Fig. 15a). High energy density of 26.9 W h kg^{-1} at a power density of 10 kW kg^{-1}, as well as excellent cyclability, was achieved (Fig. 15b). This is due to the nanocomposites taking full advantage of both the electrical double layer capacitance from the carbon layer and the pseudocapacitance from the MnO_2 embedded inside. The excellent electrical conduction from carbon layer, the porous nature of the nanocomposites that facilitates solution infiltration and ions transport, and the graphitic carbon on the tip of the nanowires that prompts the rate capacity were believed to contribute to the excellent electrochemical performance, as shown schematically in Fig. 15c. Another MnO_2/C-PDA nanostructure, paramecium-like α-MnO_2 hierarchical hollow structure, was also used as a electrochemical capacitor.[85] The specific capacitance was 554.3 F g^{-1} and 379 F g^{-1} at current rates of 1 A g^{-1} and 5 A g^{-1}, respectively. The structure also possessed good cyclability with capacitance retention of 97.9 % for 5000 cycles at 1 A g^{-1}.

d) As transparent conductive electrodes and photoelectrochemical electrodes. The rising interests on flexible devices, such as touch screens and displays, solar cells, organic light-emitting diodes and sensors, demand the invention of advanced flexible transparent and conductive films.[108, 109] For these applications, the film is required to be highly electrically conductive, mechanically strong with controllable thickness, cost effective, easy to prepare with scalability, and transparent for some applications. Compared with other counterparts, such as indium tin oxide, metal nanowires, CNTs, and graphene, DOPA-derived carbon thin film features in all the above requirements. This is due to its mild preparation condition, strong affinity to solid surfaces to form coating with adjustable thickness, and its layered structure. C-PDA thin films have been used as source-drain electrodes and flexible photodetectors.[60] For source-drain electrodes, the semiconducting polymer CDT-BTZ-C16 was drop-cast onto the C-PDA thin film-on-SiO_2/Si pattern electrodes. A high hole mobility of 0.8 cm^2 V^{-1} S^{-1} was achieved, 8 times higher than that of gold-based source-drain electrodes due to the decreased charge injection barrier of C-PDA-based electrodes compared with that of gold-based electrodes. For flexible photodetectors, C-PDA thin film was patterned to polyethylene terephthalate (PET) or PDMS substrate. The optical transmittance ranged from 92.8 to 53.5 % depending on the film thickness. A mixture of poly(3-hexylthiophene) (P3HT) and phenyl-C61-butyric acid methylester (PCBM) was then spin-coated onto the above C-PDA thin film-on-PET (or PDMS) electrodes (Fig. 16a_1~a_3). Linear current-voltage (I-V) behavior was observed, and the current increased markedly upon the light irradiation with power of about 20 mW cm^{-2} (Fig. 16b). The bending and even rolling of the flexible electrodes still delivered similar I-V behavior (Fig. 16c).

Due to the reduction and anchor capability of PDA, C-PDA thin film was also used to assist the decoration of ZnO nanorod arrays with Ag nanoparticles for photoelectrochemical application.[86] Compared with pristine ZnO nanorods, the light absorption was significantly enhanced for the C-PDA assisted Ag-decorated ZnO. The enhancement is due to the localized plasmonic effect from the small Ag nanoparticles as well as the extra visible light absorption from the C-PDA layer. As the photoanode, the short circuit current density, maximum photo current conversion efficiency, and lifetime are 1.8 mA cm^{-2}, 3.9 %, and 3.07 mA cm^{-2} at 500 seconds, respectively. These are higher than those of pristine ZnO nanorods and other reportedAg-ZnO-based photoanodes due to the enhanced light harvesting, the facilitated charge transport, and electron-hole recombination inhibition from the integrated effect of Ag nanoparticles and electrically conductive C-PDA thin layer.

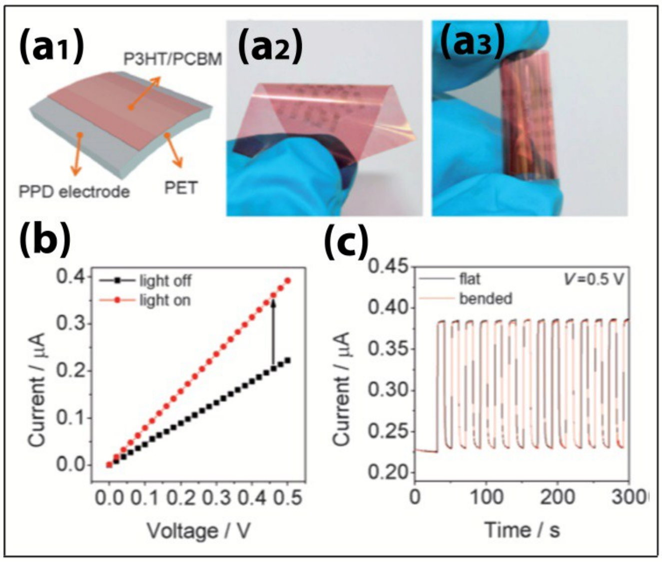

Fig. 16 (a_1-a_3) Flexible photodetector on PET substrate with C-PDA thin film as the electrode, (b) I–V characteristics of the photodetector and (c) the on/off characteristics of the photodetector in the flat and bent states [reprinted with permission from ref. [60]. Copyright 2013, John Wiley and Sons].

5.2 Applications in catalysis

The oxygen reduction reaction (ORR) is a very important process for energy conversion and storage devices, such as fuel cells and lithium air batteries. Catalysts are critically required to initiate and hold the reaction which is naturally sluggish. Many carbonaceous materials, such as mesoporous carbon,[110] graphitic carbon,[111] and N-doped CNTs,[112] have been studied as catalysts for ORR. C-PDA nanostructures have recently been reported as a promising candidate. Besides the mild preparation condition, as well as the facile control of the morphology, the graphitic structure ensures high electrical conductivity, and the inherent N doping (pyridinic N and graphitic N) enhances the electrochemical activity. It has been reported that the graphitic N increases the limiting current density and the pyridinic N improves the onset potential in the case of ORR.[113] Pure C-PDA sub-micrometer spheres (SMS) were prepared by K. Ai, et al. and used as electrode directly without any pre-treatment. Compared with traditional phenol/formaldehyde resin (PFR) SMS, the C-PDA spheres possess more positive cathodic ORR peak and onset potential, -0.218 V and -0.1 V, respectively, indicating an enhanced catalytic activity (Fig. 17a_1 and a_2).[59] . As a follow-up work, X. Yang et al. investigated the ORR property of PDA-derived micro/mesoporous nitrogen-doped carbon multilayer assemblies. The product prepared at temperature of 600 °C

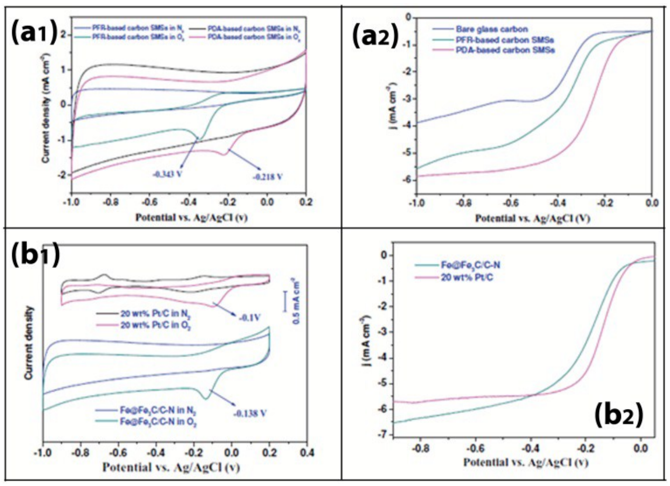

Fig. 17 (a$_1$) CV plots and (a$_2$) polarization curves of C-PDA and PFR-derived carbon SMS, (b$_1$) CV plots and (b$_2$) polarization curves of Fe@Fe$_3$C/C-N and the commercial 20 wt% Pt/C. [reprinted with permission from ref. [59]. Copyright 2012, John Wiley and Sons.]

exhibits superior electrocatalytic activity, in terms of onset potential (+0.92 V vs. RHE), number of electron transferred, the current density (10.54 mA cm^2 at +0.57 V vs. RHE), and stability, to other reference carbon materials.[63] Furthermore, nitrogen- and boron-co-doped core-shell carbon nanoparticles were prepared from PDA by J. Ahmed et al. and used as metal-free catalysts for ORR in microbial fuel cells. The co-existence of nitrogen and boron dopants creates an oxygen adsorption mechanism and a four-electron-dominated reaction pathway for the as-prepared catalyst, leading to reduced over-potential and increased current density. The microbial fuel cells showed a maximum power density of ~642 mW m^{-2}.[67]

Pt and carbon-supported Pt-based hybrids are conventional electrocatalytic candidates.[114, 115] Using DOPA at starting material, Pt@C-PDA@silica hybrids were used as anode catalyst of polymer electrolyte membrane fuel cells (PEMFCs). In such hybrids, the N-doped carbon offers excellent electrical conduction. The electrocatalytic activity of Pt can thus be maximized by the accommodation function of silica to water molecules, as well as the electrical conduction of C-PDA, resulting in a high power density of 0.55 W cm^{-2},[77] which is higher than that of commercial Pt-based PEMFCs.

As ORR catalyst, Pt-based catalysts suffer from high cost, scarcity, methanol crossover effect and poor durability. C-PDA-supported nonprecious metals offer a promising alternative. Besides the high electrical conductivity and good catalytic activity of C-PDA itself, the catechol and N-H groups in DOPA/PDA offer the opportunity to synergistically incorporate other active components facilely. K. Ai et al. investigated the ORR catalytic activity of Fe@Fe$_3$C-loaded N-doped C-PDA SMS (Fe@Fe$_3$C/C-N) in O$_2$-saturated 0.1 M KOH. The catalytic activity was further enhanced compared with pure C-PDA SMS (Fig. 17b), which is indicated by the more positive cathodic ORR peak and onset potential, 0.128 V and 0 V, respectively.[59] Through complexation route, our group formulated a one-pot approach to Fe$_3$O$_4$/C-PDA hollow nanospheres. The results show that these hollow nanospheres exhibit high onset and half-wave potentials, high current density, high selectivity for four-electron transfer pathway, superior electrocatalytic durability, and methanol tolerance compared with commercial Pt/C catalysts.[82] This is due to the high content of pyridinic and graphitic N, the graphitized C-PDA shell, the high surface area and existence of pores in C-PDA, and the synergistic effect of doped N and Fe$_3$O$_4$ nanoparticles.

Owing to its graphitic structure, as well as significant amount of pyridinic N and graphitic N, C-PDA also possesses chemical catalytic activity. The N-doped porous carbon obtained from PDA and nano-CaCO$_3$ as source and template, respectively, was used as an electrocatalyst towards reduction of nitrobenzene and oxidation of hydrazine (N$_2$H$_4$).[65] The porous carbon exhibits high peak current of -191 μA and low over-potential of -0.62 V due to the high specific surface area and large amount of doped nitrogen. In the reduction of N$_2$H$_2$, the oxidation peak current of above 200 μA and over-potential of 0.41 V were achieved. The Au@C yolk-shell monodisperse spherical nanocomposites were used as a catalyst for the reduction of 4-nitrophenol by NaBH$_4$ to 4-aminophenol.[54] UV/Vis spectra show that with the presence of An@C spheres, the reduction occurs quickly, showing their great potential as stable and highly active nanocatalysts. Another Au/C-PDA composite fully reduces 4-nitrophenol into 4-aminophenol within 4 min,[42] which indicates its higher catalytic activity than pure Au nanoparticles. By transitional metal-mediated polymerization of dopamine and subsequent annealing, Ni/C-PDA was formed on graphene and used as catalyst to reduce *p*-nitrophenol in *p*-aminophenol.[43] Owing to the unique structure, including large specific area, mesopores, high Ni content, and efficient interaction between Ni and carbon, the reduction can be finished within 80 min with the catalytic assistance of Ni/C-PDA/graphene hybrid. The catalytic activity could remain after eight cycles, showing the good stability.

5.3 Applications in sensing

The sensitivity of electronic properties of carbon materials to the surrounding gases or liquids, for instance, the change of resistance upon adsorption or desorption, renders C-PDA nanostructures promising candidates for sensors. PDA-derived hollow nitrogen-doped carbon microspheres (HNCMS) were used to electrochemically determine uric acid (UA), dopamine (DOPA), and ascorbic acid (AA) simultaneously.[55] The working electrode was prepared through casting HNCMS suspension onto surface of glassy carbon (GC) electrode followed by drying. It was claimed that the catalytic activities towards the oxidation of UA, AA, and DA were improved at the HNCMS/GC electrode. The simultaneous determination of UA, AA, and DA from HNCMS/GC electrode is more effective than that from CNTs/GC electrode due to the larger separation of the oxidation peak potentials of UA, AA, and DA. Hydrothermally prepared C-PDA dots were also used as sensing platform for turn-off detection of Fe^{3+}.[62] The capability is due to the fact that the hydroquinone units on the surface of the carbon dots can be oxidized by Fe^{3+} to form quinine species, leading to the quenching of the fluorescence of the carbon dots. The formed carbon dots/Fe^{3+} system is further employed to probe DOPA since the fluorescence of the carbon dots can be re-activated by adding DOPA to the system. High sensitivity, with detection limit of 0.32 μM and 68 nM for Fe^{3+} and DOPA, respectively, and good selectivity were achieved for the detection.

The introduction of hetero-elements alters the electronic and chemical properties of C-PDA-based hybrids, which brings new features to the system for sensing the targets. Cyclodextrins (CD) were introduced into Au@C-PDA hollow nanospheres based on the formation of Au-S bond. The high host-guest recognition and water-solubility of CD synergize with excellent electrochemical properties and large surface area of C-PDA, as well as excellent electrocatalytic activity of Au, bringing good electrochemical sensing capability. The hybrid was applied in the simultaneous electrochemical sensing of *o*-dihydroxybenzene (*o*-DHB) and *p*-dihydroxybenene (*p*-DHB).[88] Low detection limits, 0.01 and 0.02 μM for *o*-DHB and *p*-DHB, respectively, were achieved with high selectivity, good reproducibility, and good stability.

5.4 Applications as adsorbents

Besides the aforementioned application areas, C-PDA and its hybrids also show good performance in some other areas. Magnetic C-PDA particles were used to capture peptides and remove 2, 4, 6-trichlorophenol (TCP). The unique hydrophobic interactions between microspheres and peptides allow rapid capture of low-abundant peptides from complex biological samples. The captured peptides can be easily separated from the solution using a magnet due to the magnetic feature of the microspheres. The great potential of such microspheres in extraction and enrichment of peptides from complex biological samples was demonstrated.[70] Magnetic mesoporous carbon and flowerlike magnetic mesoporous carbon were used to remove TCP from an aqueous solution. The large surface area of the mesoporous carbon, about 220 m^2 g^{-1}, offers a large amount of adsorption sites for TCP, for instance, the adsorption capacities are as high as 117 and 610 mg g^{-1} for the TCP initial concentration of 10 and 100 mg L^{-1}, respectively.[79] Similarly for the flowerlike carbon, the equilibrium adsorption capacity is 210 mg g^{-1} at initial TCP concentration of 20 mg L^{-1} and increases to 587 mg g^{-1} at 100 mg L^{-1}.[80] The adsorption is dependent on the solution pH, ionic strength, the temperature, and initial concentration of TCP.

6. Concluding remarks and outlook

PDA is a unique functional material that has many advantages as carbon source, including its mild preparation condition, its strong affinity to virtually any solid surface, the ease of controlling the coating thickness, its abundant functional groups that allow diverse secondary functionalization, and its abilities to complex with various transition metal species and simultaneously reduce some of these metal species. The conversion of PDA to carbon via straightforward heat treatment in inert environment came into sight only five years ago; however, such simple conversion has brought many benefits. Firstly, the carbon yield is as high as ~60 wt%, and the resultant C-PDA has graphite-like layered structures and is intrinsically doped with pyridinic and graphitic N. The doped N induces defects and structural disorder that in general favours electrochemical process. Secondly, C-PDA is highly electrically conductive; its conductivity is comparable to that of multilayer graphene. This ensures its function as a conductive agent. Thirdly, utilizing the strong affinity of PDA, C-PDA coating can be easily created on active materials to provide protection and electrical conduction. C-PDA nanostructures could be obtained in template-free environment or upon coating onto the templates. Pre-/post-incorporation of other materials into C-PDA nanostructures is also feasible. Moreover, the complexation between transition metal species and the catechol groups in DOPA offers a facile one-pot solution to form C-PDA/metal (or metal oxides) nanocomposites. The C-PDA-based nanocomposites obtained using these routes have been explored for various applications, such as energy storage/conversion, sensing, catalysis, water treatment, etc., and shown promising properties.

Considering the rising demands for carbon-based functional nanocomposites, the potential of this unique carbon source is worthy of being further explored. At present, the complexation capability of dopamine has not been widely utilized for one-pot fabrication of C-PDA/transitional metal (or metal oxide) nanocomposites because the complexation mechanisms have not been clarified; the mechanism actually may differ from one type of transition metal species to another. This is an interesting subject for further investigation, which may lead to new routes for facile fabrication of novel functional nanocomposites. In addition, so far, the formation of C-PDA-based nanocomposites is mainly by carbonization of PDA on surface of inorganic nanostructures or incorporation/in-situ formation of inorganic nanostructures in porous/hollow C-PDA structures. A recent research shows that dopamine can also be intercalated into two-dimensional (2D) nanosheets, such as MoS_2, and thermally converted to N-doped graphene-like nanosheets in a confined interlayer space.[96] This strategy may be further extended to utilize dopamine to create Van de Waals heterostructures composed of alternately arranged highly conductive N-doped graphene-like layer and other types of 2D nanomaterials, which may exhibit fascinating properties for many functional applications. Despite the promising applications of C-PDA in various fields, challenges remain. The major challenge is that the polymerization mechanism of dopamine and chemical structure of PDA have not yet been fully clarified. In addition, the structure and properties of C-PDA are highly dependent on its preparation conditions, such as the polymerization methods and conditions used, which affect the PDA structure and morphology, as well as annealing conditions. Thus, to establish a clear guideline for rational design of C-PDA-based nanostructures for targeted applications, more efforts have to be spent on understanding of dopamine polymerization and PDA carbonization processes.

Notes and references

1. M. Terrones, A. R. Botello-Mendez, J. Campos-Delgado, F. Lopez-Urias, Y. I. Vega-Cantu, F. J. Rodriguez-Macias, A. L. Elias, E. Munoz-Sandoval, A. G. Cano-Marquez, J.-C. Charlier and H. Terrones, *Nano Today*, 2010, **5**, 351-372.
2. R. S. Edwards and K. S. Coleman, *Nanoscale*, 2013, **5**, 38-51.
3. N. M. Mubarak, E. C. Abdullah, N. S. Jayakumar and J. N. Sahu, *J. Ind. Eng. Chem.*, 2014, **20**, 1186-1197.
4. E. Frank, L. M. Steudle, D. Ingildeev, J. M. Spoerl and M. R. Buchmeiser, *Angew. Chem. Int. Ed.*, 2014, **53**, 5262-5298.
5. G. Ciric-Marjanovic, I. Pasti, N. Gavrilov, A. Janosevic and S. Mentus, *Chem. Papers*, 2013, **67**, 781-813.
6. Y. S. Chun and D. S. Lim, *J. Ceramic Soc. Jpn*, 2014, **122**, 577-585.
7. S. Dutta, A. Bhaumik and K. C. W. Wu, *Energy Environ. Sci.*, 2014, **7**, 3574-3592.
8. S. Y. Lim, W. Shen and Z. Gao, *Chem. Soc. Rev.*, 2015, **44**, 362-381.
9. S. Rondeau-Gagne and J.-F. Morin, *Chem. Soc. Rev.*, 2014, **43**, 85-98.
10. M.-M. Titirici, R. J. White, N. Brun, V. L. Budarin, D. S. Su, F. del Monte, J. H. Clark and M. J. MacLachlan, *Chem. Soc. Rev.*, 2015, **44**, 250-290.
11. L. Sun, L. Wang, C. Tian, T. Tan, Y. Xie, K. Shi, M. Li and H. Fu, *RSC Adv.*, 2012, **2**, 4498-4506.
12. Z. Yang, H. G. Nie, X. Chen, X. H. Chen and S. M. Huang, *J. Power Sources*, 2013, **236**, 238-249.
13. C. N. R. Rao, K. Gopalakrishnan and A. Govindaraj, *Nano Today*, 2014, **9**, 324-343.
14. Y. Xue, B. Wu, Q. Bao and Y. Liu, *Small*, 2014, **10**, 2975-2991.
15. H. Wang, T. Maiyalagan and X. Wang, *ACS Catal.*, 2012, **2**, 781-794.
16. Y. Tan, W. Deng, Y. Li, Z. Huang, Y. Meng, Q. Xie, M. Ma and S. Yao, *J. Phys. Chem. B*, 2010, **114**, 5016-5024.
17. R. Ouyang, H. Lei, H. Ju and Y. Xue, *Adv. Funct. Mater.*, 2007, **17**, 3223-3230.
18. S. Kobayashi and A. Makino, *Chem. Rev.*, 2009, **109**, 5288-5353.
19. H. Lee, S. M. Dellatore, W. M. Miller and P. B. Messersmith, *Science*, 2007, **318**, 426-430.
20. T. Luczak, *Electrochim. Acta*, 2008, **53**, 5725-5731.
21. N. F. Della Vecchia, R. Avolio, M. Alfe, M. E. Errico, A. Napolitano and M. d'Ischia, *Adv. Funct. Mater.*, 2013, **23**, 1331-1340.
22. S. Hong, Y. S. Na, S. Choi, I. T. Song, W. Y. Kim and H. Lee, *Adv. Funct. Mater.*, 2012, **22**, 4711-4717.
23. M. d'Ischia, A. Napolitano, V. Ball, C.-T. Chen and M. J. Buehler, *Acc. Chem. Res.*, 2014, **47**, 3541-3550.
24. V. Ball, D. Del Frari, V. Toniazzo and D. Ruch, *J. Colloid Interface Sci.*, 2012, **386**, 366-372.
25. F. Bernsmann, V. Ball, F. Addiego, A. Ponche, M. Michel, J. J. d. A. Gracio, V. Toniazzo and D. Ruch, *Langmuir*, 2011, **27**, 2819-2825.
26. F. Yu, S. Chen, Y. Chen, H. Li, L. Yang, Y. Chen and Y. Yin, *J. Mol. Struct.*, 2010, **982**, 152-161.
27. D. R. Dreyer, D. J. Miller, B. D. Freeman, D. R. Paul and C. W. Bielawski, *Langmuir*, 2012, **28**, 6428-6435.
28. J. Kong, W. A. Yee, L. Yang, Y. Wei, S. L. Phua, H. G. Ong, J. M. Ang, X. Li and X. Lu, *Chem. Commun.*, 2012, **48**, 10316-10318.
29. Y. Liu, K. Ai, J. Liu, M. Deng, Y. He and L. Lu, *Adv. Mater.*, 2013, **25**, 1353-1359.
30. S. H. Ku, J. Ryu, S. K. Hong, H. Lee and C. B. Park, *Biomater.*, 2010, **31**, 2535-2541.
31. P. Meredith and T. Sarna, *Pigm. Cell Res.*, 2006, **19**, 572-594.
32. W. J. Barreto, S. Ponzoni and P. Sassi, *Spectrochim. Acta A*, 1999, **55**, 65-72.
33. W. Osak, K. Tkacz, H. Czternastek and J. Slawinski, *Biopolym.*, 1989, **28**, 1885-1890.
34. M. M. Jastrzebska, H. Isotalo, J. Paloheimo and H. Stubb, *J. Biomater. Sci. Polym. Ed.*, 1995, **7**, 577-586.
35. A. B. Mostert, B. J. Powell, F. L. Pratt, G. R. Hanson, T. Sarna, I. R. Gentle and P. Meredith, *Proc. Natl. Acad. Sci. U. S. A.*, 2012, **109**, 8943-8947.
36. O. Z. Fisher, B. L. Larson, P. S. Hill, D. Graupner, N.-K. Mai-Thi, N. S. Kehr, L. De Cola, R. Langer and D. G. Anderson, *Adv. Mater.*, 2012, **24**, 3032-3036.
37. L. Wang, D. Wang, Z. Dong, F. Zhang and J. Jin, *Nano Lett.*, 2013, **13**, 1711-1716.
38. L. Q. Xu, W. J. Yang, K.-G. Neoh, E.-T. Kang and G. D. Fu, *Macromolecules*, 2010, **43**, 8336-8339.
39. M. Hu and B. Mi, *Environ. Sci. Technol.*, 2013, **47**, 3715-3723.
40. H. Seonki, L. Joon Seok, R. Jungki, L. Sahng Ha, L. Dong Yun, K. Dong-Pyo, P. Chan Beum and L. Haeshin, *Nanotechnol.*, 2011, **22**, 494020.
41. H. Y. Son, J. H. Ryu, H. Lee and Y. S. Nam, *Macromol. Mater. Eng.*, 2013, **298**, 547-554.
42. Z. Ma, X. Jia, J. Hu, F. Zhou and B. Dai, *RSC Adv.*, 2014, **4**, 1853-1856.
43. L. Yang, J. Kong, D. Zhou, J. M. Ang, S. L. Phua, W. A. Yee, H. Liu, Y. Huang and X. Lu, *Chem. Eur. J.*, 2014, **20**, 7776-7783.
44. A. Avdeef, S. R. Sofen, T. L. Bregante and K. N. Raymond, *J. Am. Chem. Soc.*, 1978, **100**, 5362-5370.
45. J. Monahan and J. J. Wilker, *Chem. Commun.*, 2003, DOI: 10.1039/b301052j, 1672-1673.
46. M. J. Sever, J. T. Weisser, J. Monahan, S. Srinivasan and J. J. Wilker, *Angew. Chem. Int. Ed.*, 2004, **43**, 448-450.
47. W. J. Barreto, R. A. Ando, P. S. Santos and W. P. Silva, *Spectrochim. Acta A*, 2007, **68**, 612-618.
48. N. Holten-Andersen, M. J. Harrington, H. Birkedal, B. P. Lee, P. B. Messersmith, K. Y. C. Lee and J. H. Waite, *Proc. Natl. Acad. Sci. U. S. A.*, 2011, **108**, 2651-2655.
49. Z. Xu, *Sci. Rep.*, 2013, **3**.
50. T. Sarna, W. Froncisz and J. S. Hyde, *Arch. Biochem. Biophys.*, 1980, **202**, 304-313.
51. W. Froncisz, T. Sarna and J. S. Hyde, *Arch. Biochem. Biophys.*, 1980, **202**, 289-303.
52. F. Bernsmann, A. Ponche, C. Ringwald, J. Hemmerle, J. Raya, B. Bechinger, J.-C. Voegel, P. Schaaf and V. Ball, *J. Phys. Chem. C*, 2009, **113**, 8234-8242.
53. X. Yu, H. Fan, Y. Liu, Z. Shi and Z. Jin, *Langmuir*, 2014, **30**, 5497-5505.
54. R. Liu, S. M. Mahurin, C. Li, R. R. Unocic, J. C. Idrobo, H. Gao, S. J. Pennycook and S. Dai, *Angew. Chem. Int. Ed.*, 2011, **50**, 6799-6802.

55. C. Xiao, X. Chu, Y. Yang, X. Li, X. Zhang and J. Chen, *Biosens. Bioelectron.*, 2011, **26**, 2934-2939.
56. G. W. Zajac, J. M. Gallas, J. Cheng, M. Eisner, S. C. Moss and A. E. Alvaradoswaisgood, *Biochim. Biophys. Acta*, 1994, **1199**, 271-278.
57. J. M. Gallas, K. C. Littrell, S. Seifert, G. W. Zajac and P. Thiyagarajan, *Biophys. J.*, 1999, **77**, 1135-1142.
58. H. Li, L. Shen, K. Yin, J. Ji, J. Wang, X. Wang and X. Zhang, *J. mater. Chem. A*, 2013, **1**, 7270-7276.
59. K. Ai, Y. Liu, C. Ruan, L. Lu and G. Lu, *Adv. Mater.*, 2013, **25**, 998-1003.
60. R. Li, K. Parvez, F. Hinkel, X. Feng and K. Muellen, *Angew. Chem. Int. Ed.*, 2013, **52**, 5535-5538.
61. J. Kong, W. A. Yee, Y. Wei, L. Yang, J. M. Ang, S. L. Phua, S. Y. Wong, R. Zhou, Y. Dong, X. Li and X. Lu, *Nanoscale*, 2013, **5**, 2967-2973.
62. K. Qu, J. Wang, J. Ren and X. Qu, *Chem.-Eur. J.*, 2013, **19**, 7243-7249.
63. X. Liu, H. Zhu and X. Yang, *J. Power Sources*, 2014, **262**, 414-420.
64. J. Yan, L. Yang, M.-F. Lin, J. Ma, X. Lu and P. S. Lee, *Small*, 2013, **9**, 596-603.
65. L. Yan, X. Bo, Y. Zhang and L. Guo, *Electrochim. Acta*, 2014, **137**, 693-699.
66. Y. Liang, H. Liu, Z. Li, R. Fu and D. Wu, *J. Mater. Chem. A*, 2013, **1**, 15207-15211.
67. S. Zhong, L. Zhou, L. Wu, L. Tang, Q. He and J. Ahmed, *J. Power Sources*, 2014, **272**, 344-350.
68. J. Kong, X. Yao, Y. Wei, C. Zhao, J. M. Ang and X. Lu, *RSC Adv.*, 2015, **5**, 13315-13323.
69. J. H. Kong, C. Y. Zhao, Y. F. Wei, S. L. Phua, Y. L. Dong and X. H. Lu, *J. Mater. Chem. A*, 2014, **2**, 15191-15199.
70. G. Cheng, M.-D. Zhou and S.-Y. Zheng, *ACS Appl. Mater. Interfaces*, 2014, **6**, 12719-12728.
71. H. Jiang, L. Yang, C. Li, C. Yan, P. S. Lee and J. Ma, *Energy Environ. Sci.*, 2011, **4**, 1813-1819.
72. L. Tan, L. Pan, C. Cao, B. Wang and L. Li, *J. Power Sources*, 2014, **253**, 193-200.
73. F. Han, W.-C. Li, C. Lei, B. He, K. Oshida and A.-H. Lu, *Small*, 2014, **10**, 2637-2644.
74. W. Xie, S. Li, S. Wang, S. Xue, Z. Liu, X. Jiang and D. He, *ACS Appl. Mater. Interfaces*, 2014, **6**, 20334-20339.
75. X. Yao, J. Kong, C. Zhao, D. Zhou, R. Zhou and X. Lu, *Electrochim. Acta*, 2014, **146**, 464-471.
76. C. Zhang, H. Li, N. Ping, G. Pang, G. Xu and X. Zhang, *RSC Adv.*, 2014, **4**, 38791-38796.
77. S. Seok, I. Choi, K. G. Lee, B. G. Choi, K. J. Park, J. Y. Park, O. J. Kwon, S. J. Lee and D. H. Kim, *RSC Adv.*, 2014, **4**, 42582-42584.
78. B. Ding, W. C. Tang, G. Ji, Y. Ma, P. Xiao, L. Lu and J. Y. Lee, *J. Power Sources*, 2014, **265**, 239-245.
79. S. Wang, H. Niu, T. Zeng, X. Ma, Y. Cai and X. Zhao, *Crystengcomm*, 2014, **16**, 5598-5607.
80. S. Liu, S. Li, H. Niu, T. Zeng, Y. Cai, C. Shi, B. Zhou, F. Wu and X. Zhao, *Microp. Mesop. Mater.*, 2014, **200**, 151-158.
81. N. Liu, H. Wu, M. T. McDowell, Y. Yao, C. Wang and Y. Cui, *Nano Lett.*, 2012, **12**, 3315-3321.
82. D. Zhou, L. Yang, L. Yu, J. Kong, X. Yao, W. Liu, Z. Xu and X. Lu, *Nanoscale*, 2015, **7**, 1501-1509.
83. S. Chen, M. L. Gordin, R. Yi, G. Howlett, H. Sohn and D. Wang, *Phys. Chem. Chem. Phys.*, 2012, **14**, 12741-12745.
84. H. Zhang, L. Zhou, O. Noonan, D. J. Martin, A. K. Whittaker and C. Yu, *Adv. Funct. Mater.*, 2014, **24**, 4337-4342.
85. Z. Wen, W. She, Y. Li and R. Che, *J. Mater. Chem. A*, 2014, **2**, 20729-20738.
86. Y. Wei, J. Kong, L. Yang, L. Ke, H. R. Tan, H. Liu, Y. Huang, X. W. Sun, X. Lu and H. Du, *J. Mater. Chem. A*, 2013, **1**, 5045-5052.
87. X.-C. Liu, G.-C. Wang, R.-P. Liang, L. Shi and J.-D. Qiu, *J. Mater. Chem. A*, 2013, **1**, 3945-3953.
88. G. Zhu, Y. Yi, H. Sun, K. Wang, Z. Han and X. Wu, *J. Mater. Chem. B*, 2015, **3**, 45-52.
89. M. J. Harrington, A. Masic, N. Holten-Andersen, J. H. Waite and P. Fratzl, *Science*, 2010, **328**, 216-220.
90. J. J. Wilker, *Angew. Chem. Int. Ed.*, 2010, **49**, 8076-8078.
91. H. Zeng, D. S. Hwang, J. N. Israelachvili and J. H. Waite, *Pro. Natl. Acd. Sci.*, 2010, **107**, 12850-12853.
92. M. Krogsgaard, M. A. Behrens, J. S. Pedersen and H. Birkedal, *Biomacromol.*, 2013, **14**, 297-301.
93. N. Holten-Andersen, G. E. Fantner, S. Hohlbauch, J. H. Waite and F. W. Zok, *Nat. Mater.*, 2007, **6**, 669-672.
94. N. Holten-Andersen, T. E. Mates, M. S. Toprak, G. D. Stucky, F. W. Zok and J. H. Waite, *Langmuir*, 2009, **25**, 3323-3326.
95. X. Yao, C. Zhao, J. Kong, H. Wu, D. Zhou and X. Lu, *Chem. Commun.*, 2014, **50**, 14597-14600.
96. C. Zhao, J. Kong, L. Yang, X. Yao, S. L. Phua and X. Lu, *Chem. Commun.*, 2014, **50**, 9672-9675.
97. J. R. Dahn, *Phys. Rev. B*, 1991, **44**, 9170-9177.
98. D. Billaud, F. X. Henry and P. Willmann, *Mater. Res. Bull.*, 1993, **28**, 477-483.
99. M. Inaba, H. Yoshida, Z. Ogumi, T. Abe, Y. Mizutani and M. Asano, *J. Electrochem. Soc.*, 1995, **142**, 20-26.
100. T. Ohzuku, Y. Iwakoshi and K. Sawai, *J. Electrochem. Soc.*, 1993, **140**, 2490-2498.
101. S. Flandrois and B. Simon, *Carbon*, 1999, **37**, 165-180.
102. E. M. Lotfabad, J. Ding, K. Cui, A. Kohandehghan, W. P. Kalisvaart, M. Hazelton and D. Mitlin, *ACS Nano*, 2014, **8**, 7115-7129.
103. R. Mukherjee, A. V. Thomas, D. Datta, E. Singh, J. Li, O. Eksik, V. B. Shenoy and N. Koratkar, *Nat. Commun.*, 2014, **5**, 3710.
104. J. R. Dahn, T. Zheng, Y. Liu and J. S. Xue, *Science*, 1995, **270**, 590-593.
105. D. P. Dubal, O. Ayyad, V. Ruiz and P. Gomez-Romero, *Chem. Soc. Rev.*, 2015, **44**, 1777-1790.
106. L. G. H. Staaf, P. Lundgren and P. Enoksson, *Nano Energy*, 2014, **9**, 128-141.
107. Z. N. Yu, L. Tetard, L. Zhai and J. Thomas, *Energy Environ. Sci.*, 2015, **8**, 702-730.
108. D. S. Hecht, L. B. Hu and G. Irvin, *Adv. Mater.*, 2011, **23**, 1482-1513.
109. A. Kumar and C. W. Zhou, *ACS Nano*, 2010, **4**, 11-14.
110. W. Yang, T.-P. Fellinger and M. Antonietti, *J. Am. Chem. Soc.*, 2011, **133**, 206-209.
111. R. Liu, D. Wu, X. Feng and K. Muellen, *Angew. Chem. Int. Ed.*, 2010, **49**, 2565-2569.
112. K. Gong, F. Du, Z. Xia, M. Durstock and L. Dai, *Science*, 2009, **323**, 760-764.
113. L. Lai, J. R. Potts, D. Zhan, L. Wang, C. K. Poh, C. Tang, H. Gong, Z. Shen, J. Lin and R. S. Ruoff, *Energy Environ. Sci.*, 2012, **5**, 7936-7942.

114. Y. G. Zhao, J. J. Liu, Y. H. Zhao and F. Wang, *Phys. Chem. Chem. Phys.*, 2014, **16**, 19298-19306.

115. M. C. S. Escano, *Nano Res.*, 2015, **8**, 1689-1697.